Biophysical Journal
Article

Biophysical Society

# Complex Phase Behavior of GUVs Containing Different Sphingomyelins

Daniel Balleza,[1] Andrea Mescola,[1] Nathaly Marín–Medina,[2] Gregorio Ragazzini,[1,3] Marco Pieruccini,[1] Paolo Facci,[4] and Andrea Alessandrini[1,3,*]

[1]Istituto Nanoscienze CNR, S3, Modena, Italy; [2]Departamento de Física, Universidad de Los Andes, Bogotá, Colombia; [3]Dipartimento di Scienze Fisiche, Matematiche e Informatiche, Università di Modena e Reggio Emilia, Modena, Italy; and [4]CNR – Istituto di Biofisica, Genova, Italy

ABSTRACT Understanding the lateral organization of biological membranes plays a key role on the road to fully appreciate the physiological functions of this fundamental barrier between the inside and outside regions of a cell. Ternary lipid bilayers composed of a high and a low melting temperature lipid and cholesterol represent a model system that mimics some of the important thermodynamical features of much more complex lipid mixtures such as those found in mammal membranes. The phase diagram of these ternary mixtures can be studied exploiting fluorescence microscopy in giant unilamellar vesicles, and it is typically expected to give rise, for specific combinations of composition and temperature, to regions of two-phase coexistence and a region with three-phase coexistence, namely, the liquid-ordered, liquid-disordered, and solid phases. Whereas the observation of two-phase coexistence is routinely possible using fluorescence microscopy, the three-phase region is more elusive to study. In this article, we show that particular lipid mixtures containing diphytanoyl-phosphatidylcholine and cholesterol plus different types of sphingomyelin (SM) are prone to produce bilayer regions with more than two levels of fluorescence intensity. We found that these intensity levels occur at low temperature and are linked to the copresence of long and asymmetric chains in SMs and diphytanoyl-phosphatidylcholine in the lipid mixtures. We discuss the possible interpretations for this observation in terms of bilayer phase organization in the presence of sphingolipids. Additionally, we also show that in some cases, liposomes in the three-phase coexistence state exhibit extreme sensitivity to lateral tension. We hypothesize that the appearance of the different phases is related to the asymmetric structure of SMs and to interdigitation effects.

## INTRODUCTION

Understanding the lateral organization of biological membranes could be extremely relevant to grasp some aspects of their functional role. Many of the mechanical and chemical stimuli that affect cell behavior must somehow interact with the cell membrane, and the physical-chemical properties of this barrier could contribute to signal transduction (1). Biophysicists usually exploit different kinds of model systems of the biological membrane to shed light on the fundamental physical aspects ruling its behavior (2–4). Lipids are one of the main constituents and structure-determining elements of biological membranes, and the most common model systems are composed of two, three, or even four different types of lipids (5–9). Moreover, these model systems can be assembled in the form of monolayers, liposomes, supported lipid bilayers (SLBs), or black lipid membranes (2,4). As thermodynamic structures, lipid bilayers might present different phases characterized by order/disorder of the hydrophobic chains and by solid or liquid lateral dynamics of lipid molecules. The relevance of model systems has recently been highlighted by the evidence that ternary lipid mixtures composed by a high-melting-temperature (high $T_m$) lipid, a low-melting-temperature (low $T_m$) lipid, and cholesterol, assembled in giant unilamellar vesicles (GUVs), show a thermodynamic behavior very similar to that of giant plasma membrane vesicles (10). Typically, the phase diagram for ternary mixtures is characterized by the occurrence of a large region in which two immiscible liquid phases coexist, named liquid-disordered ($L_d$) and liquid-ordered ($L_o$) phases (11–14). Immiscibility

*Submitted September 5, 2018, and accepted for publication December 20, 2018.*

*Correspondence: andrea.alessandrini@unimore.it

Daniel Balleza and Andrea Mescola contributed equally to this work.

Daniel Balleza's present address is Department of Chemistry ICET, Universidad Autonoma de Guadalajara, Lomas del Valle, Zapopan, Jalisco, Mexico.

Marco Pieruccini's present address is CNR Institute for Microelectronics and Microsystems, Bologna, Italy.

Editor: Simon Scheuring.

https://doi.org/10.1016/j.bpj.2018.12.018

© 2019 Biophysical Society.

is ascribed to the different distribution of cholesterol, which shows a higher affinity for the high $T_m$ lipids, especially if they are represented by sphingolipids (15). The biological relevance in this case is related to the presence of the $L_o$ phase, which has been connected to the "lipid-raft hypothesis" in biological membranes (16). The formation of lateral heterogeneities in a lipid bilayer could be in fact a lipid-based mechanism for the compartmentalization of membrane proteins, and it could be connected to fundamental biochemical processes (17,18). Apart from the liquid-liquid coexistence region, the phase diagram for ternary lipid mixtures foresees the presence of a triangular three-phase coexistence area (19). This triangular region includes, along with the $L_d$ and $L_o$ phases, the solid-ordered ($S_o$) phase as well.

Ternary lipid mixtures, including sphingolipids, have been deeply studied. Both natural (frequently found in mixtures) and synthetic sphingolipids have been considered in biophysical studies. This class of lipids has a strong biological relevance because of their abundance in the external leaflet of eukaryotic cells and, in the case of mammals, because of their peculiar interaction with cholesterol (20–23). Notwithstanding their relevance and profusion of previous studies devoted to understand the thermotropic behavior of sphingolipids, several aspects are still far from being well understood, and their behavior in mixtures with other lipids is to be considered as particularly complex. Part of this complexity arises from the possible presence of acyl chain asymmetry (24–27).

Together with the sphingosine chain, many different saturated and unsaturated alkyl chains of different length, ranging from 12 to 26 carbon atoms, might be found in sphingolipids composing biological membranes (28). The two main species of natural sphingolipids contain a chain with 16 or 24 carbon atoms (C16 and C24). With their very long acyl chains, C24 sphingolipids have been observed to interact with cholesterol distinctly from C16 sphingolipids (29–31). As an example, it has been recently shown that substituting C24 with C16 sphingolipids (particularly ceramides) results in metabolic defects in mice, an effect probably related to their different interface with cholesterol (32). This outcome clearly points to the critical biological relevance of sphingolipids. In addition, the thermotropic behavior of these lipids is strongly affected by their headgroup, as well. For example, the main transition for the C24:1 ceramide occurs at 44°C, whereas the C24:1 sphingomyelin (SM), sharing the same acyl chain structure, has a transition temperature of 24°C (33). Strictly connected to the chain asymmetry of these lipids is the possibility for the acyl chains to exhibit interdigitation states (29,34–37) in which part of the acyl chain of lipids in one leaflet explores the region of the opposing one. This phenomenon is expected to be relevant for ordered phases, but its relevance also in disordered phases cannot be excluded (38). Finally, considering the strong asymmetry in the composition of the biological membranes (39), the possibility of interdigitation provides a mechanism for interleaflet coupling and confers a potentially remarkable physiological role to these kinds of lipids (40). Interdigitation could in principle also alleviate the relevant hydrophobic thickness difference between ordered and disordered phases acting as a sort of interfacial attenuation of the line tension energy cost.

Here, we studied the phase behavior of ternary lipid mixtures composed of DiPhyPC (low $T_m$), cholesterol, and different types of SMs (high $T_m$). We analyzed both natural and synthetic SMs at different molar ratios, temperatures, and lateral tensions of the bilayer. As model systems, we considered GUVs, lipid monolayers at the water-air interface, and SLBs. We used fluorescence microscopy, micropipette aspiration, atomic force microscopy (AFM), and the Langmuir trough technique coupled to fluorescence microscopy so as to highlight the presence of phase separation in both mono- and bilayers. We found that more than two fluorescence intensity levels on the surface of GUVs can appear when specific lipids are present and for particular physical parameters. This situation is interesting both because of the supposed presence of a region of three-phase coexistence in the phase diagram of ternary lipid mixtures and its elusive character when GUVs are observed by fluorescence microscopy, and because it could be evidence of a more complex phase behavior in the presence of specific SMs in the membrane with respect to other high-$T_m$ lipids. The micropipette aspiration technique (MAT) allowed us to study the effect of the lateral tension on the phase state and on the shape of domains on GUVs, taking account of an additional control parameter to temperature and composition (41–44). Likewise, we compared the effect of the lateral pressure on lipid bilayers with the effect of the surface pressure on lipid monolayers of the same composition. Interesting analogous behaviors were found pointing to a relevant role of line tension in shaping lipid bilayer domains.

## MATERIALS AND METHODS

### GUV preparation and imaging

1,2-dioleoyl-*sn*-glycero-3-phosphocholine (DOPC), 1,2-dipalmitoyl-*sn*-glycero-3-phosphocholine (DPPC), brain SM (bSM) (porcine), egg-SM, diphytanoyl-phosphatidylcholine (DiPhyPC), dihydrocholesterol (dichol), cholesterol (Chol), (24:1)SM (N-nervonoyl-D-erythro-sphingosylphosphorylcholine), (24:0)SM (N-lignoceroyl-D-erythro-sphingosylphosphorylcholine), (18:0)SM (N-stearoyl-D-erythro-sphingosylphosphorylcholine) were purchased from Avanti Polar Lipids (Alabaster, AL) and used without further purification. Texas Red-DHPE (Texas Red 1,2-Dihexadecanoyl-*sn*-Glycero-3-Phosphoethanolamine) was purchased from Thermo Fischer Scientific (Waltham, MA). Specific lipid mixtures were prepared by mixing chloroform lipid solutions in the desired amount (the lipid fractions reported in this work are molar proportions). Bovine serum albumin (BSA) was acquired from Sigma Aldrich (St. Louis, MO).

GUVs were prepared by the electroformation method with minor modifications (45). Briefly, lipid mixtures were dissolved in chloroform, and small drops (2–3 $\mu$L; 2 mg/mL lipid concentration) of this mixture were deposited on two opposing Pt wires (distance between the wires equal to

~3 mm) inside a Teflon chamber. Chloroform was initially removed by exposing the Pt wires to a continuous $N_2$ flux and then by using a vacuum pump ($10^{-2}$ mbar) for at least 30 min. The two Pt wires were then connected to an electric wave generator set to produce a sinusoidal potential difference. The Teflon chamber was then filled with a 100-mM sucrose solution and sealed using glass coverslips and vacuum grease (Dow Corning, Midland, MI). The applied electroformation protocol was as follows: 1) 10 Hz, 2.0–3.0 $V_{p\text{-}p}$ peak to peak voltage for 1 h and 30 min; 2) 5 Hz, 2–2.5 $V_{p\text{-}p}$ for 30 min; and 3) 2 Hz, 1.5 $V_{p\text{-}p}$ for 15–20 min. The vesicle formation process was performed at 50°C. As a final step, we applied a square wave at 5 Hz to promote vesicle detachment from the wires. After formation, GUVs were extracted from the Teflon chamber and suspended in a 105-mM glucose solution (in some cases, we resuspended the samples in a 200-mM glucose solution to make the vesicles more flaccid). Vesicles were then allowed to cool slowly to room temperature. In place of cholesterol, we also tested dichol. It has been suggested that dichol, especially in the case of Langmuir monolayers, is more resistant than cholesterol to oxidation (46,47). However, changing cholesterol for dichol resulted in no appreciable differences in the results of the experiments both with GUVs and monolayers.

Fluorescence microscopy was performed with an Olympus IX 70 microscope (Olympus, Tokyo, Japan). Texas Red-DHPE was included in the lipid mixtures at a molar concentration of 0.5–1% or lower. Imaging was performed at controlled temperature. A home-developed imaging chamber consisting of two cover glass slides separated by a Teflon spacer was used. A small hole was made in the spacer to insert the thermocouple probe inside the water solution. The bottom slide was pretreated with 10 mg/mL BSA to remove surface charges and to avoid strong adhesion between the bilayers and the glass, which could affect the phase behavior of the vesicles. About 200 $\mu$L of a 105-mM glucose solution was inserted into the chamber, and 50 $\mu$L of vesicle suspension was added. The chamber was sealed by vacuum grease and put in direct contact with a Peltier cell. From the opposite side, the Peltier cell was in contact with a circulating water chamber whose temperature was controlled by a circulating temperature control unit (Lauda-Brinkmann, Delran, NJ). The Peltier cell was connected to a custom-developed control unit exploiting the proportional integral derivative system of an Arduino microprocessor. The system allowed for temperature jumps as fast as 15°C/min as well as controlled cooling or heating ramps (see Fig. S1 for details).

## AFM

AFM imaging was performed with a BioScope I microscope equipped with a Nanoscope IIIA controller (Veeco Metrology, Plainview, NY). We used a custom temperature-controlled stage based on a circulating water bath on which we could mount the BioScope head. The sample's temperature was continuously monitored by a digital thermometer Fluke 16 (Fluke, Brugherio MB, Italy) equipped with a small K-thermocouple probe (Thermocoax, Heidelberg, Germany) in direct contact with the imaging buffer. Temperature stability was within $\pm 0.3$°C of the specified temperature value. Triangular silicon nitride cantilevers (DNP-S; Bruker, Billerica, MA) with nominal spring constant of 0.32 N/m were used for tapping-mode imaging. All the images presented in this work have been obtained in tapping-mode AFM.

SLBs were prepared by the vesicle fusion technique. Briefly, small unilamellar vesicles were prepared by initially mixing the lipids in chloroform at the desired molar proportions. The chloroform was then removed by initially using a $N_2$ flux and then by keeping the lipids in vacuum for at least 1 h. The lipids were then resuspended in a 450 mM KCl, 100 mM phosphate-buffered saline, 10 mM $CaCl_2$ (pH 7) solution (the high ionic strength of the buffer favors the formation of SLBs). The lipid suspension was then sonicated at ~40°C, and 70 $\mu$L were deposited onto a freshly cleaved mica sheet (SPI Supplies/Structure Probe, West Chester, PA) fixed on a polytetrafluoroethylene (Teflon) disk attached to a metal disk, incubated for 15 min at a temperature above 40°C and then the sample was extensively rinsed with the imaging buffer (150 mM KCl, 50 mM phosphate-buffered saline (pH 7)). Finally, the sample was slowly cooled to the desired imaging temperature.

## Micropipette aspiration setup

Microaspiration was performed by means of pulled glass capillaries (World Precision Instruments, Sarasota, FL) with a cylindrical shape to a final internal diameter in the order of ~10 $\mu$m. Pipettes were tip polished to ensure good membrane-pipette contact and pretreated with BSA (10 mg/mL) to avoid adhesion phenomena between the glass and vesicles. For each experiment, a micropipette was connected to a pneumatic pressure controller (MPCU-3; Lorenz, Dayton, OH) to apply pressure differences between the internal side of the pipette and the external solution at the same height with a sensitivity of 1 mm $H_2O$. The pressure difference was applied by controlling the air pressure on top of a cylindrical tube containing the same external solution and initially kept at a height to assure an initial negligible pressure difference. The vesicles were manipulated inside a homemade chamber. We assembled a specific chamber in which the solution temperature could be controlled by two Peltier cells in contact with a metallic base and, from the opposite side, with a water circuit whose temperature was controlled by a temperature control unit. See Fig. S2 for the details of the setup.

In response to pressure, the vesicle is aspirated into the pipette and the lateral applied tension can be measured by the Laplace law according to the following:

$$\Delta P = \frac{2\tau}{R_p}\left(1 - \frac{R_p}{R_v}\right), \tag{1}$$

where $\tau$ is the lateral tension in the bilayer (in N/m), $R_p$ is the internal diameter of the micropipette, $\Delta P$ is the pressure difference, and $R_v$ is the external vesicle radius.

## Langmuir monolayers

For the lipid monolayer experiments, we used a Langmuir trough (Nima Technology, Coventry, UK). Before usage, the Langmuir trough was cleaned with ethanol and chloroform and then repeatedly rinsed with distilled water until it did not show any significant increase ($\Pi < 0.2$ mN/m) in the surface pressure upon barrier closure. The trough's temperature was controlled by circulating water from a water heat bath. At open barriers (surface area = 80 $cm^2$), we injected 4–5 $\mu$L of the lipids dissolved at a concentration of 1 mg/mL in chloroform. The chloroform was allowed to evaporate for 5 min; subsequently, barriers were closed at a speed of 5–10 $cm^2$/min. The lipids contained a 0.5–1% molar proportion of Texas Red-DHPE to visualize the formation of domains by epifluorescence microscopy.

# RESULTS

## Effect of the temperature and composition on the phase behavior of GUVs

The first ternary lipid mixture that we considered was DiPhyPC/bSM/Chol 1:1:1. DiPhyPC (a branched-chained lipid) was chosen as the low $T_m$ lipid of the mixture mainly because we mostly used fluorescence microscopy to inspect the phase state of lipid bilayers, and DiPhyPC provides an elevated resistance against oxidation induced by radiation damage. DiPhyPC is a synthetic lipid that adopts the $L_o$ state

for a very large temperature range (no phase transition has been found from −120 to 120°C) (48), although an order-disorder phase transition has been described as a function of the degree of hydration (49). DiPhyPC can be considered an archetypical model for methylated lipids. This kind of lipid is present in archaebacteria conferring high stability to the membrane even in extreme temperature conditions. Methyl-branched lipids have also been found in bacteria and eukaryotic cells (some SMs have been found to include chain branching) even if their physiological role has not been completely established (50,51). The lateral methyl groups on each of the isoprenoid chains of DiPhyPC confers to this lipid the tendency to form expanded states in the bilayer with a large area-per-lipid value in comparison with normal linear acyl chains. In addition, methylated phosphatidylcholines have been shown to be more fluid than the corresponding unbranched counterparts at a given temperature (46). It has also been found that a phosphatidylcholine with two phytanoyl chains packs very poorly with cholesterol, and this behavior can have a role in the formation of $L_o$ and $L_d$ domains (47). Additionally, the methyl groups in DiPhyPC have been shown to favor a negative monolayer curvature (52,53).

bSM is a natural extract containing many different species, the dominant ones being (18:0)SM (50%) (https://avantilipids.com) and (24:1)SM (∼20%). Phase diagrams of similar ternary mixtures have been previously investigated using different techniques (27,54–57), and a phase coexistence region with two types of liquid domains has been observed. The coexistence of three phases, including also an $S_o$ phase, has remained more elusive. The occurrence of the different phases depends on temperature, but it should be kept in mind that the lateral organization of the lipid bilayer can also be influenced by properties related to line tension and membrane curvature, which are both affected by the lateral tension applied to the vesicle.

When GUVs of the ternary lipid mixture DiPhyPC/bSM/Chol 1:1:1 plus 0.5–1% molar proportion of Texas Red-DHPE are prepared by the electroformation method and imaged by fluorescence microscopy at 16°C, the population has mainly a bimodal distribution. As shown in Fig. 1, apart from a large population of vesicles presenting the usual two fluorescence intensity levels that we assign to $L_o$ and $L_d$ phases, a small group of vesicles exhibits three fluorescence levels (which from now on we will call 3-ph vesicles). Considering the intensity levels, it seems that the new appearing level has an intermediate fluorescence between the ones attributed to $L_o$ and $L_d$ phases. We also found that the probability of finding 3-ph vesicles increases upon decreasing temperature and after the vesicles have been stored for a long period (a few hours) at 4°C. Remarkably, at 12°C the percentage of vesicles with three fluorescence intensity levels is ∼7% ($n = 300$ vesicles). We then tried to follow the formation of regions with three different intensity levels by decreasing the temperature. To this aim, we

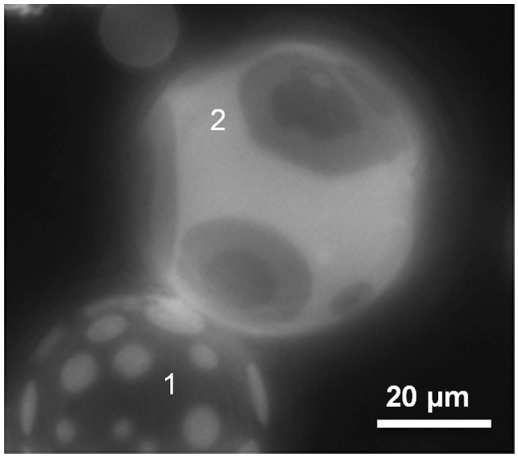


FIGURE 1 Fluorescence microscopy image of representative GUVs composed by an equimolar mixture of DiPhyPC/bSM/dichol + 1% Texas Red-DHPE at 16°C. A GUV presenting two different phases (GUV 1) and a GUV with three fluorescence intensity levels (GUV 2) are observed.

initially increased temperature to 50°C to make the liposomes completely homogeneous. According to the phase diagram for the ternary lipid system at issue or with very similar composition, at 50°C, most of the vesicles are in the homogeneous $L_d$ phase. To keep the vesicle constantly in the field of view of the camera during the cooling step, we aspirated and kept at low constant tension one uniform vesicle with a micropipette. Fig. 2 shows a sequence of snapshots of a representative 3-ph vesicle during this cooling ramp (see the corresponding Video S1). We observed that the lipid demixing starts at a temperature of 34°C producing what are typically interpreted as $L_o$ domains (*dark regions*) surrounded by the $L_d$ phase (*brighter matrix*). By further decreasing temperature, the newly formed domains tend to enlarge and coalesce. Starting from a temperature around 16°C, a third fluorescence intensity level appears in the lipid bilayer (Fig. 2 *e*). The new intensity level is intermediate between the previously observed ones, and it seems to completely surround the darkest regions. If the temperature is further decreased, we observe an increase of the area occupied by the region with the intermediate level of fluorescence intensity (see Fig. S3 for an analysis of the fluorescence intensity levels for 3-ph vesicles). Furthermore, the above described evolution can be observed when the vesicles are not grabbed by a micropipette as well (see Fig. S4), demonstrating that the behavior cannot be ascribed to the lateral tension applied by the micropipette setup. Overall, the intermediate region seems to grow mainly at the expense of the brighter one (see Fig. S5 for the quantitative analysis), and it completely wets the darkest regions. Carrer et al. (58) reported a case in which three intensity levels were observed on GUVs by fluorescence microscopy. However, in the latter case, the vesicles had four components, and the geometry of the domains strongly depended on the amount of brain ceramides in the vesicles. By

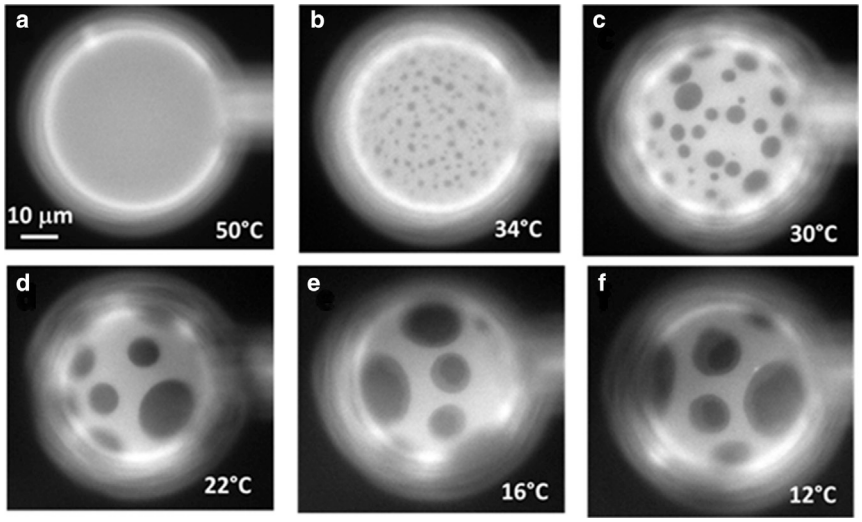


FIGURE 2 (*a–f*) Sequence of fluorescence microscopy images of a 3-ph GUV composed of an equimolar proportion of DiPhyPC/bSM/Chol (plus 1% Texas Red DHPE) for decreasing temperature values. To have an easier tracking of the vesicle during the temperature quench, the vesicle has been grabbed using a small negative pressure applied with a glass micropipette (on the *right* in the image). The same behavior has been observed for the other five vesicles.

performing fluorescence correlation spectroscopy, they were able to exclude the possibility of leaflet decoupling as an explanation for the different intensity levels. The authors attributed the intermediate level to an intermediate phase between the $L_o$ and the $L_d$ one.

We also studied the effect of a change in Chol concentration while keeping the same proportion of DiPhyPC and bSM. Our results indicate that for a Chol concentration of 25%, we never observed the third fluorescent intensity level appearance, whereas, for concentrations from 29 up to 40%, the three fluorescence intensities were always observed in a similar percentage of vesicles (see Fig. S6).

## Effect of the lateral tension

If a 3-ph GUV grabbed by a micropipette is exposed to an increasing lateral tension by increasing the negative pressure, the intermediate fluorescent region is always removed. Under such conditions, this region is transformed to round domains showing the lowest or the highest fluorescence intensity levels. An example of this behavior is reported in Fig. 3 (see Fig. S7; Video S2 for other examples). On the other hand, if temperature is increased, the removal of the intermediate level occurs mainly by the appearance of bright domains, which progressively increase their area until only two fluorescence intensity levels are left (see Fig. S8).

## AFM of SLBs

We also performed an AFM analysis on the same lipid mixture (DiPhyPC/bSM/Chol 1:1:1) prepared as an SLB. In AFM analysis of lipid bilayers, the presence of different phases is inferred by the appearance of regions with different heights (i.e., bilayer thickness). Fig. 4 shows a representative image of effects on an SLB at decreasing temperature. Starting from 25°C, we observed the presence of two height levels on the lipid bilayer, which we attribute to $L_d$ and $L_o$ phases. At 16°C, the regions surrounding the thicker domains adopt an intermediate height as evidenced in Fig. 4 *c*, which shows line sections obtained across the lines in Fig. 4, *a* and *b*. As in the case of GUVs, these data further confirm the formation of new domains upon decreasing the temperature. The fact that some domains decrease their thickness upon decreasing temperature is a strong indicator of interdigitation effects. In general, even if we have found several cases in which the behavior was like the one described in Fig. 4, this was not observed in all the SLBs having the same lipid composition. This fact is also consistent to what we observed for GUVs. Even if AFM could be very useful for the investigation of lipid bilayer phases given that nanodomains are easily detected, it is possible to have leaflet decoupling in SLBs (59). However, it is very difficult to know if the different occurring domains are due to phases that span the whole bilayer or if they involve just one of them. We performed force spectroscopy analysis of the SLBs as well, yet the curves showed no evidence of leaflet decoupling (see Fig. S9). Under different conditions, three phases have been found on SLBs of ternary mixtures by AFM (60). In that case, it has been observed that $S_o$ regions had a lower thickness than $L_o$ areas because of the amount of Chol that is not enough to create a $L_o$ phase but is able to induce an order decrease of the $S_o$ region. This phase has been called the "disordered gel phase," and its formation is favored at low Chol concentration (10–15%) and by cooling the bilayer at a low rate (~1°C/min). In our case, the concentration of Chol is quite high (30–40%), and it should therefore disfavor the appearance of this type of domain.

## Synthetic SMs

In principle, a bilayer composed by a lipid mixture containing a high-$T_m$ lipid, a low $T_m$-lipid, and Chol should be

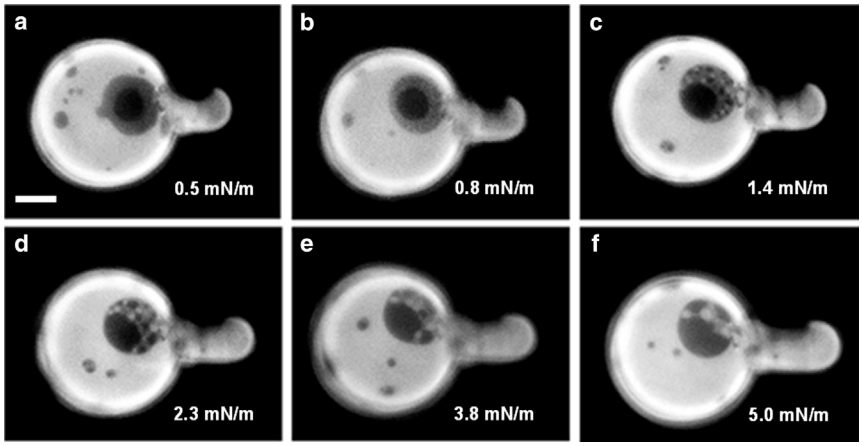


FIGURE 3 (*a–f*) Sequence of images of a typical 3-ph GUV upon increasing the lateral tension at 15°C (from 0.5 to 5 mN/m). The aspirating micropipette is to the right of the vesicle, and the increasing lateral pressure is evidenced by the growth of the vesicle projection inside the micropipette. Scale bar, 10 $\mu$m. (See Video S2.) A similar behavior has been observed for at least seven vesicles under similar circumstances.

considered equivalent to a system with five components. This is due to the fact that the membrane is composed by two separate leaflets and two types of lipids (high and low $T_m$), which cannot easily translocate from one leaflet to the other, whereas Chol is more free to diffuse transversally. In the case of GUVs prepared by electroformation, it is assumed there is no asymmetry in the lipid composition, and domains in the two leaflets are kept in register by an interleaflet coupling mechanism. Accordingly, the effective number of components should be reduced to three. However, bSM is already a mixture by itself with two main species, (18:0)SM and (24:1)SM, which represent 50 and 20% of the total composition, respectively. Hence, the appearance of three fluorescence intensity levels could also be explained by the number of components being higher than three. In particular, we hypothesized that at 16°C, the (24:1)SM component could segregate from the other bSM species giving rise to a new phase. Moreover, C24:1 chains interact differently with Chol with respect to chains with a lower number of C atoms. To understand the possible role of all species in the mixture, we firstly considered a more pure natural SM, egg-SM, which is a mixture too, yet the dominant phase, 16:0 SM, represents ~86% of the total composition. In this case, we were not able to observe the coexistence of the three fluorescence intensities (see Fig. S10). We then used synthetic SMs, starting from (18:0)SM. The mixture of DiPhyPC/(18:0)SM/Chol was not able to produce 3-ph GUVs (see Fig. S11). In addition, with (18:0)SM, the typical features of the $S_o$ phase were observed at low temperature (see Fig. S11 *b*), including dendritic domains with not rounded borders. We then moved to the second major component of the bSM mixture, specifically (24:1)SM. In this case, the percentage of 3-ph vesicles increased (up to ~15% at 12°C) ($n = 250$ vesicles). Interestingly, the presence of the intermediate fluorescence level is not strictly confined to the boundary with the darkest domains and, in many cases, it is the most abundant phase.

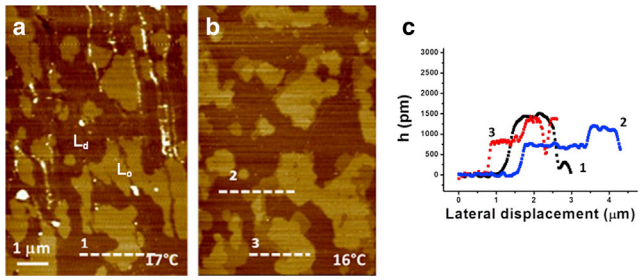


FIGURE 4 AFM images showing the phase state of a DiPhyPC/bSM/Chol 1:1:1 SLB at two different temperatures: (*a*) 17°C; (*b*) 16°C; (*c*) line sections corresponding to the dashed lines reported in (*a–b*). To see this figure in color, go online.

Different possibilities exist for the appearance of the three levels. Fig. 5 *a* shows the case in which bright domains surrounded by the intermediate level appear (type I case), whereas Fig. 5, *b* and *c* shows the case in which the darkest and intermediate fluorescence intensity regions are surrounded by the brightest region (type II case). Fig. 5 *d* shows the case in which isolated circular domains appear for each fluorescence intensity level (type III case).

It is important to note that when regions of the darkest fluorescence intensity are inside a larger domain of intermediate fluorescence level, the dark domains apparently cannot cross the border between the highest level of fluorescence and the intermediate one, a phenomenon that supports the fact that the different domains come from a single bilayer. In principle, there could be not-in-register domains present in the bilayer, which could provide an explanation for the appearance of the three fluorescence levels. Nonetheless, the analysis of domain behavior upon coalescence (see Fig. S12) confirms the fact that the three different fluorescence intensity levels must be attributed to configurations spanning the whole bilayer. Then we analyzed the behavior of the 3-ph GUVs upon variation of the temperature. Fig. 6 shows the behavior when the temperature is increased until the GUV reaches homogeneous fluorescence intensity.

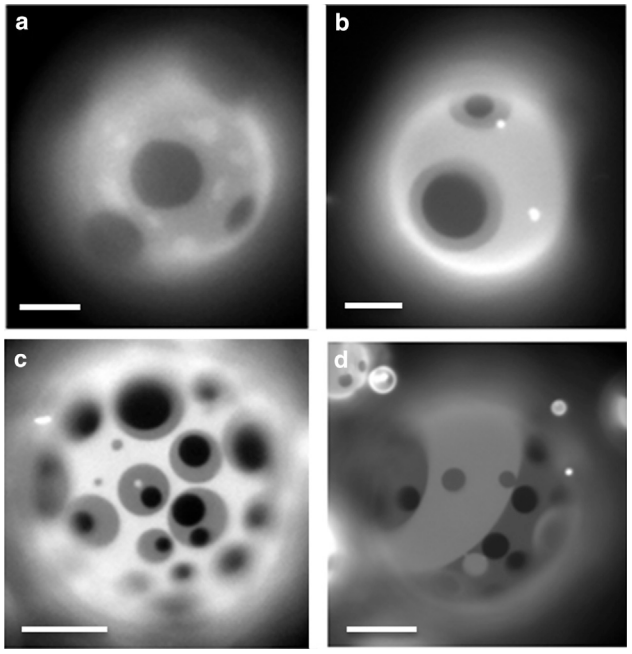


FIGURE 5 Examples of domains appearing in the case of the ternary mixture DiPhyPC/(24:1)SM/Chol 1:1:1 plus 0.5–1% Texas Red DHPE. (*a*) Appearance of the brighter and not rounded domains in the intermediate fluorescent intensity region (type I); (*b* and *c*) darkest domains completely wetted by the intermediate fluorescence intensity region (type II); (*d*) appearance of rounded domains of all the three fluorescent intensity levels (type III). Scale bar, 10 $\mu$m.

Increasing the temperature results immediately in a decrease of the line tension between the brightest and the intermediate fluorescence intensity regions as deduced from the irregular boundaries. Moreover, the two brighter phases become very similar to each other with a fading interface region, whereas the darkest regions are removed. At a temperature of ~34°C, the GUV becomes homogeneous (i.e., without any apparent lipid segregation). Fig. S13 reports also the behavior corresponding to the subsequent cooling of the same GUV down to 12°C, showing that the formation of the different regions is completely reversible. Another example of phase behavior of DiPhyPC/(24:1)SM/Chol GUVs upon temperature increase is included in Fig. S14, as well.

Considering the peculiar behavior of the DiPhyPC/(24:1) SM/Chol mixture, we analyzed different molar proportions of the three lipids. By increasing the amount of DiPhyPC with respect to (24:1)SM, keeping constant the cholesterol concentration to 33.3%, we found that for the mixture DiPhyPC/(24:1)SM/Chol 53.3/13.3/33.3, just a few vesicles clearly showed the 3-ph condition, whereas at a temperature <20°C, most of the vesicles showed only two fluorescence levels with multilobe-shaped domains (see Fig. S15). It is to be remarked that the fluorescence intensity differences could be so small as to be undetectable. For the mixture DiPhyPC/(24:1)SM/Chol 13.3/53.3/33.3, we were not able to find 3-ph GUVs, and they typically showed just two regions (bright domains on a dark background). According to these results, a similar amount of DiPhyPC and (24:1) SM is required for the appearance of the three domains. We also exchanged (24:1)SM for (24:0)SM. In this case, three fluorescence intensity levels with a behavior similar to that observed for (24:1)SM were detected (see Fig. S16), yet the 3-ph state was typically detected up to 35°C. It is to be stressed that (24:0)SM has a higher transition temperature with respect to (24:1)SM (61), but, at the same time, (24:1)SM and (24:0)SM have different properties, with (24:0)SM more similar to (18:0)SM than (24:1)SM.

## AFM of SLBs with synthetic SM

We next obtained AFM images of SLBs prepared from small unilamellar vesicles that were of the DiPhyPC/(24:1)SM/Chol 1:1:1 ternary mixture. Previous AFM studies showed that in presence of ethanol, supported bilayers can adopt, for specific lipid compositions, an interdigitated phase (62). Nevertheless, interdigitation has also been observed by AFM for pure DHPC bilayers in the absence of ethanol (33,63). The appearance of the new phase in AFM experiments is deduced from the lower thickness of the interdigitated domains (62,64). Interestingly, when the interdigitated domains are studied by polarized total-internal-reflection fluorescence microscopy in SLBs, a contrast inversion is obtained by changing the light polarization. This behavior is related to the orientation of the Texas Red DHPE fluorescence probe. By changing the light polarization from s- to p-, the interdigitated and the $L_d$ regions invert their relative fluorescence intensity. For the s-polarization (parallel to the substrate), which is the case closely resembling the conditions found in epifluorescence microscopy (65), the interdigitated phase is brighter than the $L_d$ phase. This aspect stresses again the fact that the association of the fluorescence intensity with the order parameter should be evaluated with care.

AFM can provide directly the analysis of the bilayer thickness, offering another way to reveal the order of different domains in the lipid bilayer. Fig. 7 shows the results we obtained at low temperature for the specific mixture we used. At higher temperatures, the lipid bilayer appears uniform, whereas at 20°C, the formation of thicker domains occurs. By further decreasing temperature, starting from ~12°C, another type of domain appears. These new domains are characterized by a circular or semicircular region of lower thickness, and the region inside this border has a height that is just a fraction of a nanometer thicker than the surrounding bilayer (see Fig. S17). This height difference is very small (~0.2–0.3 nm), which could be undetectable in many cases. This very small height difference points to very tiny differences in the lipid chain order of the different domains. The absolute height of the bilayers is ~4–4.5 nm. This value is not consistent with a bilayer

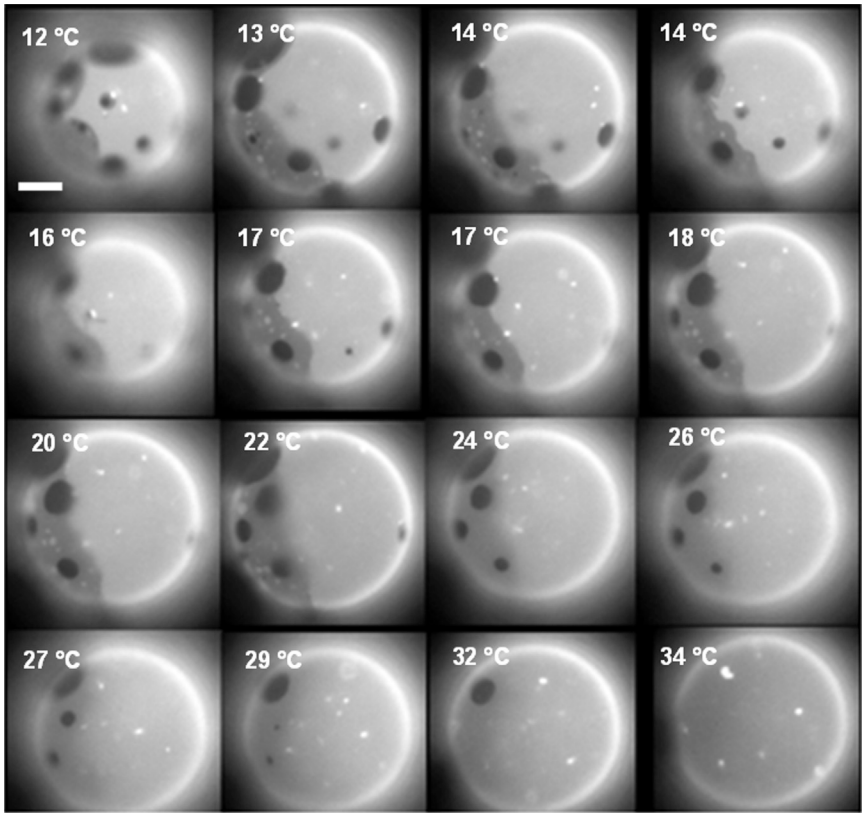


FIGURE 6 Sequence of fluorescence microscopy images of a DiPhyPC/(24:1)SM/Chol + 0.5% Texas Red DHPE as the temperature is increased from 12 to 34°C. The border between the brightest and the intermediate fluorescence intensity regions gradually disappears without apparently changing the relative area, whereas the darkest regions shrink until they disappear. Scale bar, 10 $\mu$m.

composed of 24.1 SM in the straight conformation in both leaflets unless we consider interdigitation effects. Hence, in general terms, at low temperatures, three phases are observed in SLB (see Fig. S18 for other examples).

## Effect of lateral tension on vesicles containing (24:1)SM

Another interesting aspect of this mixture is the appearance of modulated phases at low temperature (8–9°C) involving the brightest and the intermediate fluorescence intensity regions (see Fig. S19). The appearance of this particular phase is highly favored by releasing the lipid bilayer lateral tension via an increase of the external osmotic pressure, which is obtained by an increment of the sugar concentration outside the vesicle. In other cases, the formation of modulated phases is observed while increasing the temperature (see Fig. S20) just after the decrease of the line tension between the intermediate and brightest fluorescence intensity regions where the trend of the line tension is deduced from the increasing irregularity of the borders separating the two regions. The modulated phases start with linear structures and then tend to small rounded regions. Considering the dependence of the modulated phase on the tension in the lipid bilayer, we concentrated on the effect of the lateral tension on the appearance and the shapes of the domains for the DiPhyPC/(24:1)SM/Chol mixture. Fig. 8 shows the effects on a type I vesicle grabbed by the micropipette at increasing lateral tension (see Video S3). The vesicle initially showed the presence of bright domains in

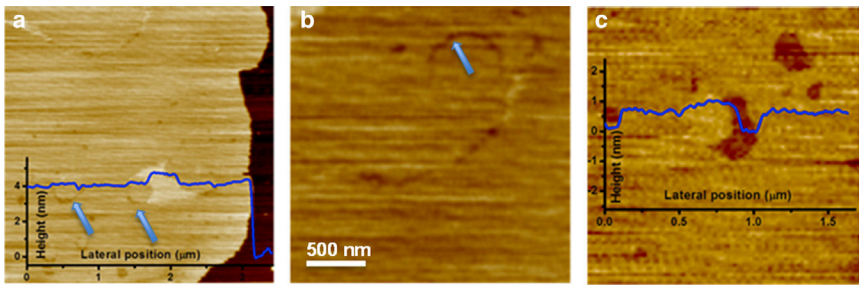


FIGURE 7 (*a–c*) AFM images of DiPhyPC/(24:1)SM/Chol 1:1:1 SLBs obtained at 12°C. In (*a*) and (*c*), the line sections on specific regions of the sample are reported evidencing the presence of more than two height levels. In (*a*) and (*b*), the presence of annular regions with lower height with respect to the surrounding bilayer is highlighted by arrows. To see this figure in color, go online.

a background, which can be associated with the intermediate intensity level. These domains typically show a large fluctuation of their borders with an estimated line tension of (0.066 ± 0.035) pN (see Supporting Materials and Methods for the details of the calculation). At higher resolution, some of these domains show the presence of modulations with stripes of different fluorescence intensity inside the domains with the highest fluorescence intensity (Fig. 8 *a*), whereas, in other cases, no structures were observed (see Fig. S21; Videos S4 and S5 for other examples). Fig. S22 reports the detailed shape changes of a domain when the lateral tension of the GUV is increased by MAT. The quantitative analysis of the area of the different domains shows that the increase of the lateral tension corresponds to an increase of the region characterized by the brightest fluorescence intensity as well as a decrease of the area with the darkest fluorescence intensity. This behavior points to the connection between the brightest region and an area with greater disorder than the latter one.

Fig. 8 shows that upon an increase of the pressure difference between the inside and the outside of the micropipette, a strong reorganization of the domains occurs. The stripes inside the bright domains increase their width until they fuse in dark subdomains near the boundary of the bright domain. At the same time, the bright regions assume a higher fluorescence intensity and a quarter moon-like shape. Notably, the shape changes are fully reversible (see Videos S3, S4, and S5) and occur over a lateral tension range going from $\sim 10^{-2}$ to 1 mN/m where the vesicle bending fluctuations are dominant. From these results, we speculate that the shape changes are mainly related to the removal of fluctuations and not to a molecular area increase in the lipid bilayer (stretching component). According to this evidence, it seems the modulated phases are ascribable to different spontaneous fluctuations of the curvatures from different domains in the bilayer. In the case of type II vesicles in which the background region is the brightest one, the lateral tension increase produces a negligible effect on the shape of the domains (see Fig. S23).

## Langmuir monolayers of DiPhyPC/(24:1)SM/Chol

The shapes adopted by the domains in the case of the DiPhyPC/(24:1)SM/Chol 1:1:1 mixture upon changes in the GUV lateral tension are reminiscent of what happens in the case of lipid monolayers when three different phases (i.e., gas, liquid expanded, and liquid condensed) are present at the air-water interface and the lateral pressure is varied. Theoretical approaches that are able to explain what happens to domains in the three-phase coexistence region have been developed (66–68). Accordingly, we investigated the possible equivalence of GUVs under the effect of an increasing lateral tension and monolayers in a Langmuir trough for which we controlled the lateral pressure. Fig. 9 reports examples of the similarities we observed. We found changes in the domain shapes when the bilayer lateral tension was increased (greater molecule-to-molecule distance), which corresponds to a lateral pressure decrease in the Langmuir trough (increase of area-per-molecule). Theories developed for the analysis of lipid monolayers ascribe most of the observed behavior to effects related to the competition between line tension among the different

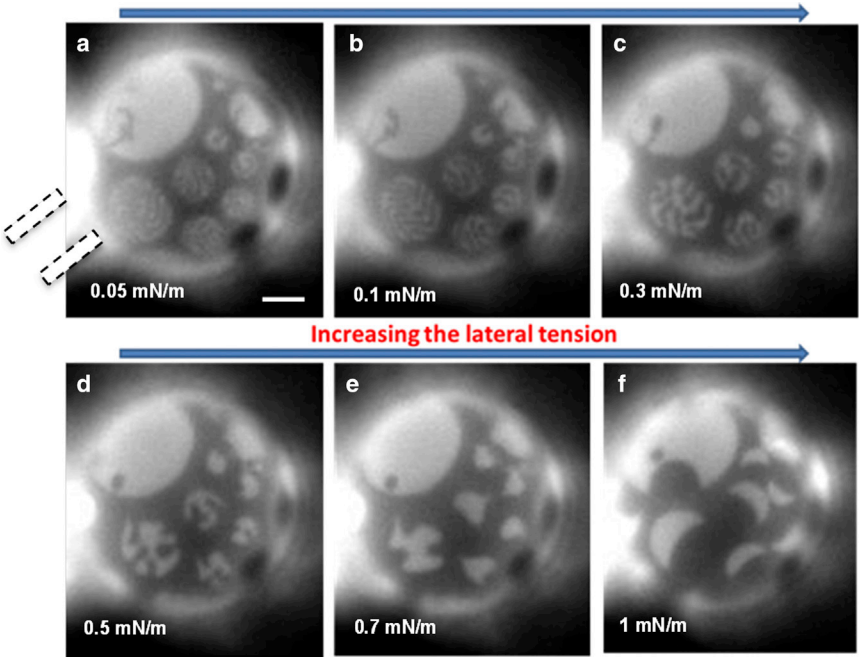


FIGURE 8 (*a–f*) Fluorescence microscopy images of a DiPhyPC/(24:1)SM/Chol + 1% DHPE Texas Red undergoing a lateral tension increase. The micropipette is on the left of the image (*dashed lines* in the first frame). See also Video S3. Scale bar, 10 $\mu$m. To see this figure in color, go online.

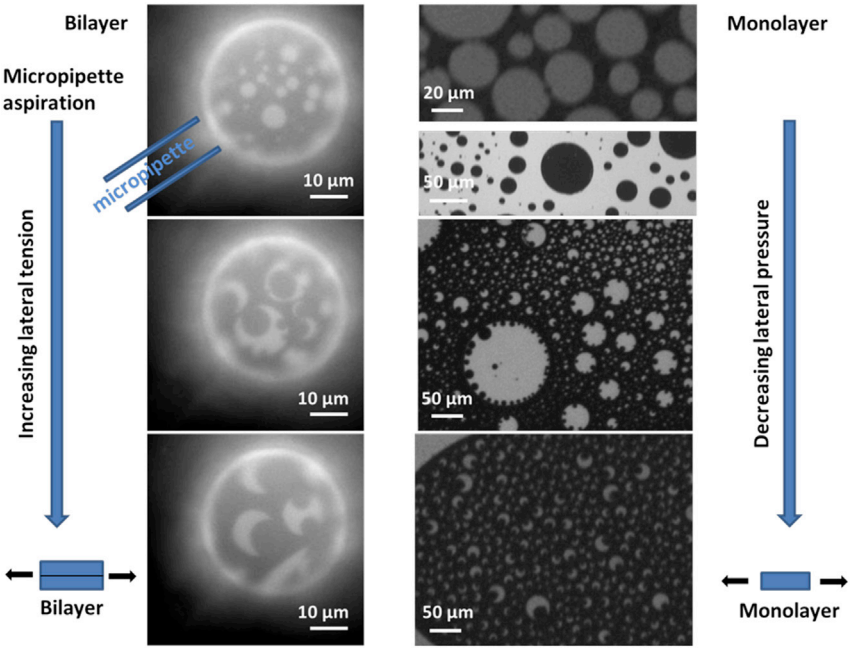


FIGURE 9 Analogies between the appearance of domains in a DiPhyPC/(24:1)SM/Chol 1:1:1 + 1% Texas Red DHPE GUV as a function of the applied lateral tension (*left column*) in a MAT setup and domains of the same lipid composition in a Langmuir monolayer upon decreasing the lateral pressure (*right column*). The lateral tension in the GUV on the left column ranges from 0.3 to 0.8 mN/m moving from the upper to the lower case, whereas the lateral tension in the monolayer is 12 mN/m in the first two images and less than 0.5 mN/m in the remaining two cases. To see this figure in color, go online.

domains, dipole repulsion, and wetting phenomena (66). The wetting phenomena in Langmuir monolayers presenting three different phases have been largely investigated (68). Upon changes in the values of both the dipole density difference among the different domains and the line tension, wetting and dewetting transitions associated with large shape changes of the domains occur (see for example Figs. 2 and 3 in (68)). Similar changes take place when the above parameters are held constant and the areas of different domains are modified (68).

## DISCUSSION

Unraveling the phase behavior of sphingolipids represents a difficult task because of the many different types of molecular structure they have, the different types of bonds they form with other lipids in the bilayer, and the presence of very asymmetric acyl chains (69). Sphingolipids have been associated to the raft hypothesis for lipid bilayers because, in model systems, they typically form complexes with Chol in the $L_o$ domain, suggesting a clue relevance of sphingolipids in plasma membranes. Here, we found that a mixture including a natural SM extract, like bSM or synthetic analogs ((24:1)SM and (24:0)SM), together with cholesterol and DiPhyPC, can give rise to a phase behavior in which three fluorescence intensity levels might appear. Domains with an intermediate fluorescence intensity appear when the temperature is decreased, completely surrounding darkest domains in the case of bSM. Considering that the new domains with an intermediate fluorescence intensity level are formed at the interface between the brightest and darkest domains, we exclude the possibility that we are observing the formation of the typical $S_o$ phase. In fact, the $S_o$ phase would be expected to form in the central part of an already dark region. Moreover, AFM images of SLBs of ternary mixtures containing bSM showed the formation of new domains with intermediate thickness at low temperature (~16°C). At first, we tentatively attributed the formation of the new domains to the fact that bSM is already a mixture (the two main components are (18:0) and (24:1) SMs). It is not unusual to observe three different types of domains when more than three types of molecule are present in a lipid mixture. This is observed when, for example, ceramides are added to ternary lipid mixtures (58). Nonetheless, the experiments we performed with synthetic SMs clearly showed that the appearance of the intermediate phase is not strictly related to the presence of more than three components. When a purely ternary mixture including the synthetic (24:1) or (24:0)SM lipids and DiPhyPC is considered, three fluorescence intensity levels are still obtained. Our experiments clearly showed that these specific SMs, in combination with DiPhyPC, are responsible for this three-phases phenomenon. However, whereas in the case of bSM, the intermediate phase always wet the darkest regions, in the case of (24:1) or (24:0)SM, we found that the intermediate phase can also be present in the form of isolated domains, pointing to a possible different explanation for the formation of the different domains.

We used the MAT to study the behavior of different phases when the lateral tension in the bilayer is increased. It has been recently reported that the osmotic differences between the inside and outside regions of GUVs strongly affect the shape and size of $L_o$ and $L_d$ domains (70). It is to be stressed that temperature decrease induces on its

own an increase of the lateral tension of the GUV because of the fact that the area decrease of the lipid bilayer prevails over volume decrease (71,72). Accordingly, effects related to the lateral tension increase could be evident also when temperature is decreased. In particular, any undulated or ripple phases present in the vesicle will be removed simply by increasing the lateral tension resulting in a planar structure. Actually, the role of lateral tension on the phase behavior of lipid bilayers has been already considered both in theoretical (41,73) and experimental investigations (42–44,74). In principle, considering the 2D version of the Clausius-Clapeyron law, an increase of lateral tension should favor more expanded phases. For example, it has been found that the demixing temperature from a completely $L_d$ phase to the coexistence of $L_o$ and $L_d$ phases decreases upon an increase of the lateral tension (43). Moreover, theoretical analysis showed that a lateral tension increase produces a line tension rise when domains of different hydrophobic thickness are present (73). The variation of the line tension in the case of a domain thicker than the surrounding lipids (like in the case of a lipid raft) has been predicted to be appreciable. This effect is related to the curvature and elastic moduli of the domains and to the tilt and splay deformations at the borders of the domains. In this context it is also possible that the molecular details of the lipids could be equally important to determine the extent to which line tension is affected by the lateral pressure. In light of all these considerations, the intermediate phase in the case of bSM cannot be ascribed to an increase of the lateral tension in the bilayer during the cooling step because the transformation of a bright region into an intermediate fluorescence intensity region should correspond to an increase of the lateral order. Furthermore, we noticed that the intermediate region is removed by an increase of the lateral tension applied by the micropipette.

The line tension increase could induce the coalescence of nanodomains, which are not optically detectable. These dark $L_o$ nanodomains on the bright $L_d$ background would result in an intermediate fluorescence intensity level. Thus, when temperature is decreased, the height difference between the $L_o$ and $L_d$ domains could increase up to the point at which a wetting layer made by $L_o$ nanodomains is energetically favored (see Fig. S9). The coalescence of nanodomains into microdomains allows the possibility to observe them by fluorescence microscopy. A similar explanation has been hypothesized previously by Li and Cheng (75) even in the absence of Chol (DLPC/DPPC GUVs prepared at high (1M) sucrose concentration or DLPC/DPPC plus DOPG GUVs were used). This mechanism could in principle explain the effect observed for bSM upon lateral pressure increase.

If we consider the coexistence of three different phases as suggested by AFM, we have to understand their nature. It has been shown that (24:1)SM has a very broad and complex differential scanning calorimetry thermogram, and it is not prone to form well-ordered domains (76). Different temperatures have been associated to (24:1)SM bilayer reorganizations; from high to low temperature, two reorganizations occur at 25 and 16°C even if the exact nature of these transitions has not been clarified. Even in the case of (24:0)SM, a complex thermotropic behavior with multiple transitions has been observed, being strongly dependent on the hydration degree of the molecules and the thermal history of the sample. Notably, these behaviors have been attributed also to transitions between a tilted, partially interdigitated to an almost untilted, interdigitated gel phase at low temperatures (39.4°C), with major changes in lipid thickness (77). In general, it has been observed that for SMs with different chain length, the appearance of complex thermograms starts for chains with more than 18–20 carbon atoms. This fact coincides with the appearance of chain asymmetry in the acyl chains (33).

According to these considerations, a possible explanation for the formation of the third type of domains is given by the formation of interdigitated phases upon a temperature decrease due to the presence of the strongly asymmetric (24:1)SM species (bSM contains ~34 mol % of asymmetric molecules, including C22, and of this 34 mol %, 59% is unsaturated). The detection of the phase diagram just by fluorescence microscopy presents the problem of associating the intensity of the fluorescent emission, strictly related to the partition coefficients of the marker, to the different lipid phases (i.e., lipid order) that can be present. This is particularly critical in our case in which (24:1)SM is prone to adopt interdigitated phases at low temperature, and the partitioning of fluorescence markers in this phase is unclear. Moreover, different lipid organizations giving rise to interdigitated conditions (i.e., mixed, partial, and complete interdigitation) are possible (78), and different lipid packing is expected in different situations. Concomitantly, the fully and mixed interdigitated phases imply an increase of the lateral area and a strong decrease of the bilayer thickness. Considering AFM images, the height difference among the different domains is small (~0.5 nm), and it allows us to exclude the possibility of a complete interdigitation state. In the case of (24:1)SM, the height differences are even smaller, and if the different domains are due to interdigitation effects, the overlap of the acyl chains of the two leaflets is also very small. At the same time, the absolute thickness of the bilayers measured by AFM (~4–4.5 nm) is consistent with at least a partial interdigitation phenomenon of the chains (61). Pinto et al. (79) studied the phase behavior of (24:1) nervonoylceramide in the binary mixture with 1-palmitoyl-2-oleoyl-*sn*-glycero-3-phosphocholine. They found a complex behavior of the mixture at low temperature, which was attributed to an initial change from a mixed interdigitated gel phase to a partially interdigitated one and then to a fluid phase at increasing temperature. They also found regions of phase coexistence with lines in the phase diagram in which three phases could coexist. Similar results have been found for SM (80). Because the main phase transition

of (24:1)SM occurs at ~16–20°C and the intermediate phase appears at a very similar temperature, it is feasible to relate the appearance of the intermediate phase to a change in the organization of the (24:1)SM molecules. In this case, the first dark domains that are formed by decreasing temperature are due to the $L_o$ phase in which mainly (18:0)SM is involved, whereas (24:1)SM remains in the $L_d$ phase. At a temperature of ~16°C, (24:1)SM adopts a more ordered state, and the possible interdigitation of (24:1)SM, probably favored by the large area-per-molecule of DiPhyPC, explains the lower thickness of the newly formed $L_o$ phase with respect to the (18:0)SM related $L_o$ region as observed by AFM (see Fig. 4). This interdigitated phase could have a reduced area-per-molecule occupation, and this would explain, at least in part, the fact that the intermediate phase collapses by increasing the lateral tension.

Previous studies using the ternary mixture DOPC/(24:1)SM/Chol reported that (24:1)SM inhibits the formation of laterally heterogeneities like the formation of $L_o$ domains, yet the behavior at low temperature has not been considered (81). In the same study, it was established that exchanging (24:1)SM for (24:0)SM leads to the formation of separated domains. In this context, DiPhyPC could have a role in the interdigitation effects. Indeed, the ether derivative of DiPhyPC has been shown to form interdigitated phases, as well (63). In light of this fact, it is probable that DiPhyPC could favor the formation of interdigitated phases via SM with long chains even if it does not interdigitate when considered as a single component.

The images we obtained for the case of the DiPhyPC/(24:1 or 24:0)SM/Chol mixtures are quite similar to those reported in a work by Collins and Keller (82) in which they used a ternary mixture of DiPhyPC/DPPC/Chol in a lipid bilayer with asymmetric leaflet composition. They found three different fluorescence intensity levels, and their appearance was related to the asymmetry of the bilayer. However, they found that the three levels should be associated to bilayer spanning phases and the three intensity levels could also be found in just one leaflet. Because in our case we should have a symmetric bilayer, the reason for the appearance of the different fluorescence levels should be different. In one recent molecular dynamics investigation, it has been found that the presence of C24 SM in just one leaflet forces cholesterol to the opposite one (83). At the same time, cholesterol in the opposite leaflet is able to push C24 SM slightly out from the bilayer, and its interaction with cholesterol in the same leaflet is reduced. The asymmetric structure of the bilayer could produce bilayer spanning phases with different values of fluorescence intensity because of a nonsymmetric partitioning of the fluorophore. Accordingly, in our case, the asymmetry in leaflet composition could be a process that is induced by the presence of C24 SM. We also observed, especially in the case of a largely reduced tension of the lipid bilayer obtained by an osmotic unbalance, that modulated phases involving the two brighter regions appeared.

One interesting aspect of the domain shape in the case of the DiPhyPC/(24:1)SM/Chol mixture is its extreme dependence on the lateral tension of the bilayer. The behavior we observed in GUVs is similar to what is observed at the interface of three phases in Langmuir monolayers. The shape of the domains formed in the case of phase coexistence is finely tuned by the mutual line tension between the phases and by the area of each phase according to the Young equation. Both parameters can in turn be affected by the applied lateral tension. In the case of monolayers, a parameter ruling the wettability of different phase domain is related to both the dipole moment difference and the line tension between each pair of phases (68). For example, it is possible to induce wettability transitions in two-dimensional systems by reducing the area-per-molecule. Considering the behavior of lipid bilayers, we can hypothesize that aspects related to line tension and wetting phenomena are relevant for the shape of domains when three phases characterized by different lipid density are present simultaneously and they have very similar thicknesses. In this case, we have to consider that the main contribution of the dipole moment in ester-linked lipid membranes has to be associated with the carbonyl group of each leaflet (50). Their dipole moments are quite far from each other and, as a consequence, the possibility to be mutually neutralized becomes unlikely. Accordingly, dipole interactions should play a role in the shape of the domains in bilayers as it has been established for monolayers.

Considering all the possibilities, we hypothesize that in the presence of highly asymmetric and very long chain SMs and DiPhyPC, one $L_d$ phase and two different $L_o$ phases exist, with the latter associated to two different interdigitation states of SM. Generally, interdigitated phases are associated with gel or ordered phases, but it is not to be excluded that interdigitation can also have effects on liquid phases. The $L_d$ phase and one of the two $L_o$ phases have a very similar thickness as highlighted by our AFM results. In some cases, it is possible to have the copresence of three phases in which the shape of the domains is strongly dependent on the lateral tension in the bilayer as a result of variations in the mutual area fraction and line tension. In the case of monolayers, it has been proposed that for long acyl chains, as is the case of 24:1 ceramide, a transition from a "mushroom" to a "brush" configuration might occur by increasing the lateral pressure, like in the case of grafted polymers (24). It is not clear yet how these findings could be translated to the bilayer case, but it is to be considered that temperature and lateral tension might affect the configuration of the long acyl chains inside the bilayer.

## CONCLUSIONS

We have found that the appearance of more than two fluorescence intensity levels occurs at low temperature for ternary lipid mixtures, including the highly asymmetric

lipid (24:1) SM, a methyl-branched ester lipid, DiPhyPC, and Chol. If (24:1)SM is substituted for (24:0)SM, the three fluorescent levels are present even at higher temperature (up to 35°C). We attributed the presence of the three intensity levels to the asymmetric and very long chains of SMs and the formation of different interdigitated structures, which can favor phases with different lipid densities. This is relevant because very long chain sphingolipids (>20 C) are largely present in specialized tissues, and some functional properties of the membranes are affected if these specific lipids are lacking. Notably, we have found that when the 3-ph state is present on a GUV, the shape of domains involving the phase with the brightest fluorescence level can be strongly dependent on the lateral tension applied to the vesicle. Based on the strong similarities between the behavior of domains in the GUVs when the lateral tension is increased and domains in lipid monolayers when the surface pressure is released, we assigned a strong relevance to line tension and wetting phenomena in the organization of lipid domains in bilayers. This experimental evidence, although obtained on a model system, could have biological relevance considering the typical very low lateral tension of plasma membranes in living cells. Moreover, the complex alteration of the membrane state induced by the presence of (24:0) or (24:1)SM could be one of the reasons for their biological effect (83). Thus, the possible interdigitation of very long and asymmetric SM lipid species could contribute to the coupling of the inner and outer leaflets in biological membranes.

## SUPPORTING MATERIAL

Supporting Materials and Methods, thirty figures, and five videos are available at http://www.biophysj.org/biophysj/supplemental/S0006-3495(18)34532-6.

## AUTHOR CONTRIBUTIONS

D.B., A.M., and A.A. designed research's strategy. D.B., A.M., N.M-M., G.R., and A.A. performed experiments. All authors analyzed the data and contributed to the manuscript writing.

## REFERENCES


1. Anishkin, A., S. H. Loukin, …, C. Kung. 2014. Feeling the hidden mechanical forces in lipid bilayer is an original sense. *Proc. Natl. Acad. Sci. USA.* 111:7898–7905.
2. Mouritsen, O. G. 2011. Model answers to lipid membrane questions. *Cold Spring Harb. Perspect. Biol.* 3:a004622.
3. Mouritsen, O. G., and L. A. Bagatolli. 2015. Lipid domains in model membranes: a brief historical perspective. *Essays Biochem.* 57:1–19.
4. Simons, K., and W. L. Vaz. 2004. Model systems, lipid rafts, and cell membranes. *Annu. Rev. Biophys. Biomol. Struct.* 33:269–295.
5. Goh, S. L., J. J. Amazon, and G. W. Feigenson. 2013. Toward a better raft model: modulated phases in the four-component bilayer, DSPC/DOPC/POPC/CHOL. *Biophys. J.* 104:853–862.
6. Feigenson, G. W. 2009. Phase diagrams and lipid domains in multicomponent lipid bilayer mixtures. *Biochim. Biophys. Acta.* 1788:47–52.
7. McConnell, H. M., and M. Vrljic. 2003. Liquid-liquid immiscibility in membranes. *Annu. Rev. Biophys. Biomol. Struct.* 32:469–492.
8. Radhakrishnan, A., T. G. Anderson, and H. M. McConnell. 2000. Condensed complexes, rafts, and the chemical activity of cholesterol in membranes. *Proc. Natl. Acad. Sci. USA.* 97:12422–12427.
9. Veatch, S. L., and S. L. Keller. 2005. Seeing spots: complex phase behavior in simple membranes. *Biochim. Biophys. Acta.* 1746:172–185.
10. Veatch, S. L., P. Cicuta, …, B. Baird. 2008. Critical fluctuations in plasma membrane vesicles. *ACS Chem. Biol.* 3:287–293.
11. Ipsen, J. H., O. G. Mouritsen, and M. J. Zuckermann. 1989. Theory of thermal anomalies in the specific heat of lipid bilayers containing cholesterol. *Biophys. J.* 56:661–667.
12. Ipsen, J. H., G. Karlström, …, M. J. Zuckermann. 1987. Phase equilibria in the phosphatidylcholine-cholesterol system. *Biochim. Biophys. Acta.* 905:162–172.
13. Veatch, S. L., and S. L. Keller. 2003. Separation of liquid phases in giant vesicles of ternary mixtures of phospholipids and cholesterol. *Biophys. J.* 85:3074–3083.
14. Veatch, S. L., and S. L. Keller. 2002. Organization in lipid membranes containing cholesterol. *Phys. Rev. Lett.* 89:268101.
15. Veatch, S. L., and S. L. Keller. 2005. Miscibility phase diagrams of giant vesicles containing sphingomyelin. *Phys. Rev. Lett.* 94:148101.
16. Lingwood, D., and K. Simons. 2010. Lipid rafts as a membrane-organizing principle. *Science.* 327:46–50.
17. Rayermann, S. P., G. E. Rayermann, …, S. L. Keller. 2017. Hallmarks of reversible separation of living, unperturbed cell membranes into two liquid phases. *Biophys. J.* 113:2425–2432.
18. Phillips, R., T. Ursell, …, P. Sens. 2009. Emerging roles for lipids in shaping membrane-protein function. *Nature.* 459:379–385.
19. Clarke, J. A., J. M. Seddon, and R. V. Law. 2009. Cholesterol containing model membranes studied by multinuclear solid state NMR spectroscopy. *Soft Matter.* 5:369–378.
20. Carreira, A. C., A. E. Ventura, …, L. C. Silva. 2015. Tackling the biophysical properties of sphingolipids to decipher their biological roles. *Biol. Chem.* 396:597–609.
21. Westerlund, B., and J. P. Slotte. 2009. How the molecular features of glycosphingolipids affect domain formation in fluid membranes. *Biochim. Biophys. Acta.* 1788:194–201.
22. Ramstedt, B., and J. P. Slotte. 2002. Membrane properties of sphingomyelins. *FEBS Lett.* 531:33–37.
23. Maggio, B., M. L. Fanani, …, N. Wilke. 2006. Biophysics of sphingolipids II. Glycosphingolipids: an assortment of multiple structural information transducers at the membrane surface. *Biochim. Biophys. Acta.* 1758:1922–1944.
24. Holopainen, J. M., H. L. Brockman, …, P. K. Kinnunen. 2001. Interfacial interactions of ceramide with dimyristoylphosphatidylcholine: impact of the N-acyl chain. *Biophys. J.* 80:765–775.
25. Zhai, X., X. M. Li, …, R. E. Brown. 2006. Lactosylceramide: lateral interactions with cholesterol. *Biophys. J.* 91:2490–2500.
26. Goñi, F. M., A. Alonso, …, J. L. Thewalt. 2008. Phase diagrams of lipid mixtures relevant to the study of membrane rafts. *Biochim. Biophys. Acta.* 1781:665–684.
27. de Almeida, R. F., A. Fedorov, and M. Prieto. 2003. Sphingomyelin/phosphatidylcholine/cholesterol phase diagram: boundaries and composition of lipid rafts. *Biophys. J.* 85:2406–2416.
28. Fahy, E., S. Subramaniam, …, E. A. Dennis. 2005. A comprehensive classification system for lipids. *J. Lipid Res.* 46:839–861.
29. Jaikishan, S., and J. P. Slotte. 2011. Effect of hydrophobic mismatch and interdigitation on sterol/sphingomyelin interaction in ternary bilayer membranes. *Biochim. Biophys. Acta.* 1808:1940–1945.

30. Quinn, P. J., and C. Wolf. 2009. Thermotropic and structural evaluation of the interaction of natural sphingomyelins with cholesterol. *Biochim. Biophys. Acta.* 1788:1877–1889.

31. Quinn, P. J. 2013. Structure of sphingomyelin bilayers and complexes with cholesterol forming membrane rafts. *Langmuir.* 29:9447–9456.

32. Sas, K. M., V. Nair, …, S. Pennathur. 2015. Targeted lipidomic and transcriptomic analysis identifies dysregulated renal ceramide metabolism in a mouse model of diabetic kidney disease. *J. Proteomics Bioinform* (*Suppl. 14*):002.

33. Jiménez-Rojo, N., A. B. García-Arribas, …, F. M. Goñi. 2014. Lipid bilayers containing sphingomyelins and ceramides of varying N-acyl lengths: a glimpse into sphingolipid complexity. *Biochim. Biophys. Acta.* 1838:456–464.

34. Lewis, R. N., R. N. McElhaney, …, S. M. Gruner. 1994. Enigmatic thermotropic phase behavior of highly asymmetric mixed-chain phosphatidylcholines that form mixed-interdigitated gel phases. *Biophys. J.* 66:207–216.

35. Mehlhorn, E. I., E. Florio, …, C. W. M. Grant. 1988. Evidence that trans-bilayer interdigitation of glycosphingolipid long chain fatty acids may be a general phenomenon. *Biochim. Biophys. Acta.* 939:151–159.

36. Róg, T., A. Orłowski, …, I. Vattulainen. 2016. Interdigitation of long-chain sphingomyelin induces coupling of membrane leaflets in a cholesterol dependent manner. *Biochim. Biophys. Acta.* 1858:281–288.

37. Boggs, J. M., and K. M. Koshy. 1994. Do the long fatty acid chains of sphingolipids interdigitate across the center of a bilayer of shorter chain symmetric phospholipids? *Biochim. Biophys. Acta.* 1189:233–241.

38. Schram, V., and T. E. Thompson. 1995. Interdigitation does not affect translational diffusion of lipids in liquid crystalline bilayers. *Biophys. J.* 69:2517–2520.

39. Devaux, P. F. 1991. Static and dynamic lipid asymmetry in cell membranes. *Biochemistry.* 30:1163–1173.

40. Fujimoto, T., and I. Parmryd. 2017. Interleaflet coupling, pinning, and leaflet asymmetry-major players in plasma membrane nanodomain formation. *Front. Cell Dev. Biol.* 4:155.

41. Uline, M. J., M. Schick, and I. Szleifer. 2012. Phase behavior of lipid bilayers under tension. *Biophys. J.* 102:517–522.

42. Chen, D., and M. M. Santore. 2014. Large effect of membrane tension on the fluid-solid phase transitions of two-component phosphatidylcholine vesicles. *Proc. Natl. Acad. Sci. USA.* 111:179–184.

43. Portet, T., S. E. Gordon, and S. L. Keller. 2012. Increasing membrane tension decreases miscibility temperatures; an experimental demonstration via micropipette aspiration. *Biophys. J.* 103:L35–L37.

44. Hamada, T., Y. Kishimoto, …, M. Takagi. 2011. Lateral phase separation in tense membranes. *Soft Matter.* 7:9061–9068.

45. Dimitrov, D. S., and M. I. Angelova. 1988. Lipid swelling and liposome formation mediated by electric fields. *J. Electroanal. Chem. Interfacial Electrochem.* 253:323–336.

46. Silvius, J. R., and R. N. McElhaney. 1980. Effects of phospholipid acyl chain structure on thermotropic phase properties. 3. Phosphatidylcholines with (−), and (±)-anteiso acyl chains. *Chem. Phys. Lipids.* 26:67–77.

47. Bakht, O., P. Pathak, and E. London. 2007. Effect of the structure of lipids favoring disordered domain formation on the stability of cholesterol-containing ordered domains (lipid rafts): identification of multiple raft-stabilization mechanisms. *Biophys. J.* 93:4307–4318.

48. Lindsey, H., N. O. Petersen, and S. I. Chan. 1979. Physicochemical characterization of 1,2-diphytanoyl-sn-glycero-3-phosphocholine in model membrane systems. *Biochim. Biophys. Acta.* 555:147–167.

49. Hung, W. C., F. Y. Chen, and H. W. Huang. 2000. Order-disorder transition in bilayers of diphytanolyl phosphatidylcholine. *Biochim. Biophys. Acta.* 1467:198–206.

50. Ohashi, Y., T. Tanaka, …, Y. Nagai. 2000. Squid nerve sphingomyelin containing an unusual sphingoid base. *J. Lipid Res.* 41:1118–1124.

51. Carter, H. E., and C. B. Hirschberg. 1968. Phytosphingosines and branched sphingosines in kidney. *Biochemistry.* 7:2296–2300.

52. Shinoda, K., W. Shinoda, …, M. Mikami. 2004. Comparative molecular dynamics study of ether- and ester-linked phospholipid bilayers. *J. Chem. Phys.* 121:9648–9654.

53. Yasmann, A., and S. Sukharev. 2015. Properties of diphytanoyl phospholipids at the air-water interface. *Langmuir.* 31:350–357.

54. Veatch, S. L., and S. L. Keller. 2003. A closer look at the canonical 'Raft Mixture' in model membrane studies. *Biophys. J.* 84:725–726.

55. Konyakhina, T. M., and G. W. Feigenson. 2016. Phase diagram of a polyunsaturated lipid mixture: brain sphingomyelin/1-stearoyl-2-docosahexaenoyl-sn-glycero-3-phosphocholine/cholesterol. *Biochim. Biophys. Acta.* 1858:153–161.

56. Petruzielo, R. S., F. A. Heberle, …, G. W. Feigenson. 2013. Phase behavior and domain size in sphingomyelin-containing lipid bilayers. *Biochim. Biophys. Acta.* 1828:1302–1313.

57. Veatch, S. L., K. Gawrisch, and S. L. Keller. 2006. Closed-loop miscibility gap and quantitative tie-lines in ternary membranes containing diphytanoyl PC. *Biophys. J.* 90:4428–4436.

58. Carrer, D. C., E. Kummer, …, P. Schwille. 2009. Asymmetry determines the effects of natural ceramides on model membranes. *Soft Matter.* 5:3279–3286.

59. Seeger, H. M., G. Marino, …, P. Facci. 2009. Effect of physical parameters on the main phase transition of supported lipid bilayers. *Biophys. J.* 97:1067–1076.

60. Aufderhorst-Roberts, A., U. Chandra, and S. D. Connell. 2017. Three-phase coexistence in lipid membranes. *Biophys. J.* 112:313–324.

61. Niemelä, P. S., M. T. Hyvönen, and I. Vattulainen. 2006. Influence of chain length and unsaturation on sphingomyelin bilayers. *Biophys. J.* 90:851–863.

62. Vanegas, J. M., R. Faller, and M. L. Longo. 2010. Influence of ethanol on lipid/sterol membranes: phase diagram construction from AFM imaging. *Langmuir.* 26:10415–10418.

63. Balleza, D., A. B. Garcia-Arribas, …, F. M. Goñi. 2014. Ether- versus ester-linked phospholipid bilayers containing either linear or branched apolar chains. *Biophys. J.* 107:1364–1374.

64. Ngo, A. T., Z. J. Jakubek, …, L. J. Johnston. 2014. Membrane order parameters for interdigitated lipid bilayers measured via polarized total-internal-reflection fluorescence microscopy. *Biochim. Biophys. Acta.* 1838:2861–2869.

65. Oreopoulos, J., and C. M. Yip. 2008. Combined scanning probe and total internal reflection fluorescence microscopy. *Methods.* 46:2–10.

66. Perković, S., and H. M. McConnell. 1997. Cloverleaf monolayer domains. *J. Phys. Chem. B.* 101:381–388.

67. Heinig, P., S. Wurlitzer, …, T. M. Fischer. 2002. Stability criteria for two-dimensional wetting in monolayers. *J. Phys. Chem. B.* 106:11951–11960.

68. Khattari, Z., P. Heinig, …, T. M. Fischer. 2002. Wetting in asymmetric quasi-2D systems. *Langmuir.* 18:2273–2279.

69. García-Arribas, A. B., E. J. González-Ramírez, …, F. M. Goñi. 2017. Complex effects of 24:1 sphingolipids in membranes containing dioleoylphosphatidylcholine and cholesterol. *Langmuir.* 33:5545–5554.

70. Cornell, C. E., A. D. Skinkle, …, S. L. Keller. 2018. Tuning length scales of small domains in cell-derived membranes and synthetic model membranes. *Biophys. J.* 115:690–701.

71. Käs, J., and E. Sackmann. 1991. Shape transitions and shape stability of giant phospholipid vesicles in pure water induced by area-to-volume changes. *Biophys. J.* 60:825–844.

72. Needham, D., and E. Evans. 1988. Structure and mechanical properties of giant lipid (DMPC) vesicle bilayers from 20 degrees C below to 10 degrees C above the liquid crystal-crystalline phase transition at 24 degrees C. *Biochemistry.* 27:8261–8269.

73. Akimov, S. a., P. I. Kuzmin, …, F. S. Cohen. 2007. Lateral tension increases the line tension between two domains in a lipid bilayer membrane. *Phys. Rev. E Stat. Nonlin. Soft Matter Phys.* 75:011919.

74. Chen, D., and M. M. Santore. 2014. Three dimensional (temperature-tension-composition) phase map of mixed DOPC-DPPC vesicles: two solid phases and a fluid phase coexist on three intersecting planes. *Biochim. Biophys. Acta.* 1838:2788–2797.

75. Li, L., and J. X. Cheng. 2006. Coexisting stripe- and patch-shaped domains in giant unilamellar vesicles. *Biochemistry.* 45:11819–11826.

76. Björkqvist, Y. J., J. Brewer, …, B. Westerlund. 2009. Thermotropic behavior and lateral distribution of very long chain sphingolipids. *Biochim. Biophys. Acta.* 1788:1310–1320.

77. Maulik, P. R., and G. G. Shipley. 1996. Interactions of N-stearoyl sphingomyelin with cholesterol and dipalmitoylphosphatidylcholine in bilayer membranes. *Biophys. J.* 70:2256–2265.

78. Slater, J. L., and C. H. Huang. 1988. Interdigitated bilayer membranes. *Prog. Lipid Res.* 27:325–359.

79. Pinto, S. N., L. C. Silva, …, M. Prieto. 2008. Membrane domain formation, interdigitation, and morphological alterations induced by the very long chain asymmetric C24:1 ceramide. *Biophys. J.* 95:2867–2879.

80. Levin, I. W., T. E. Thompson, …, C. Huang. 1985. Two types of hydrocarbon chain interdigitation in sphingomyelin bilayers. *Biochemistry.* 24:6282–6286.

81. Maté, S., J. V. Busto, …, F. M. Goñi. 2014. N-nervonoylsphingomyelin (C24:1) prevents lateral heterogeneity in cholesterol-containing membranes. *Biophys. J.* 106:2606–2616.

82. Collins, M. D., and S. L. Keller. 2008. Tuning lipid mixtures to induce or suppress domain formation across leaflets of unsupported asymmetric bilayers. *Proc. Natl. Acad. Sci. USA.* 105:124–128.

83. Courtney, K. C., W. Pezeshkian, …, X. Zha. 2018. C24 sphingolipids govern the transbilayer asymmetry of cholesterol and lateral organization of model and live-cell plasma membranes. *Cell Rep.* 24:1037–1049.

**Biophysical Journal, Volume *116***

## Supplemental Information

# Complex Phase Behavior of GUVs Containing Different Sphingomyelins

**Daniel Balleza, Andrea Mescola, Nathaly Marín–Medina, Gregorio Ragazzini, Marco Pieruccini, Paolo Facci, and Andrea Alessandrini**

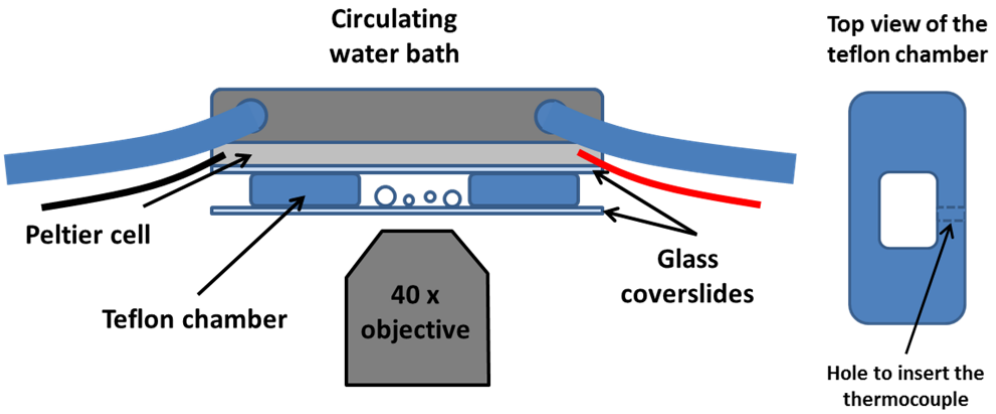


Fig. S1:Scheme of the set-up used to analyze the GUVs at different temperatures with the epifluorescence microscope. The Peltier cell is connected to a home-developed temperature controller device implementing a PID control by the Arduino Uno board. The circulating water bath is exploited as fast heat sink.

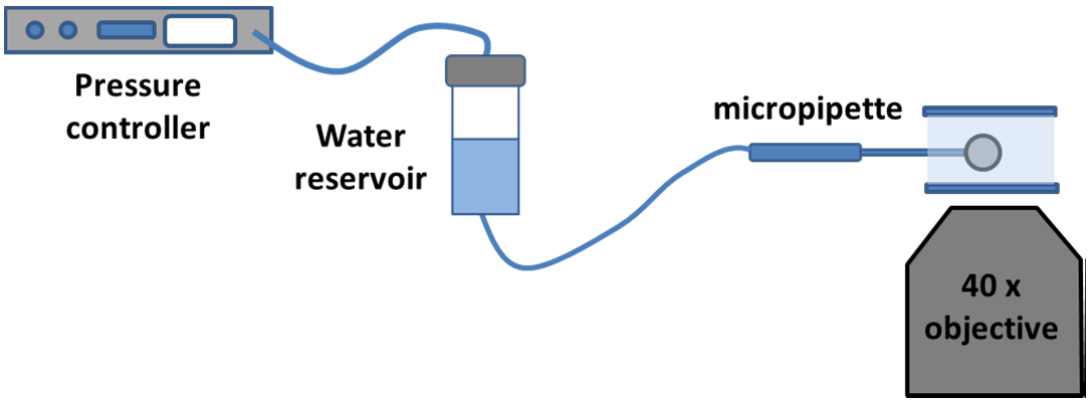


Fig. S2: Scheme of the Micropipettte aspiration set-up exploited to change the lateral tension of the GUVs. The pressure controller is used to control the pressure on top of the water reservoir. The water reservoir is connected to the micropipette.

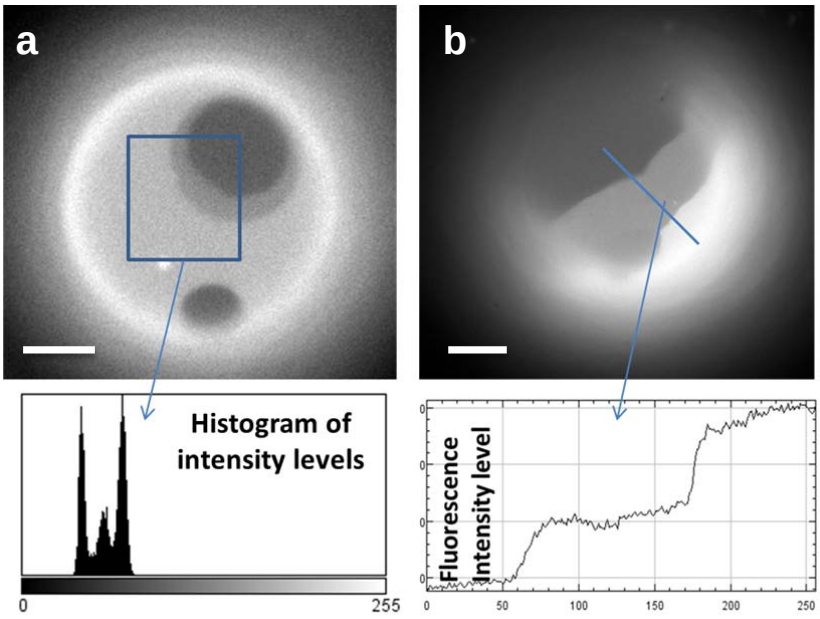


Fig. S3: Fluorescence intensity analysis (histogram of intensity levels in a) and line section in b)) for DiPhyPC/bSM/Cho 1/1/1 GUVs showing three intensity levels. (Bar = 10 µm)

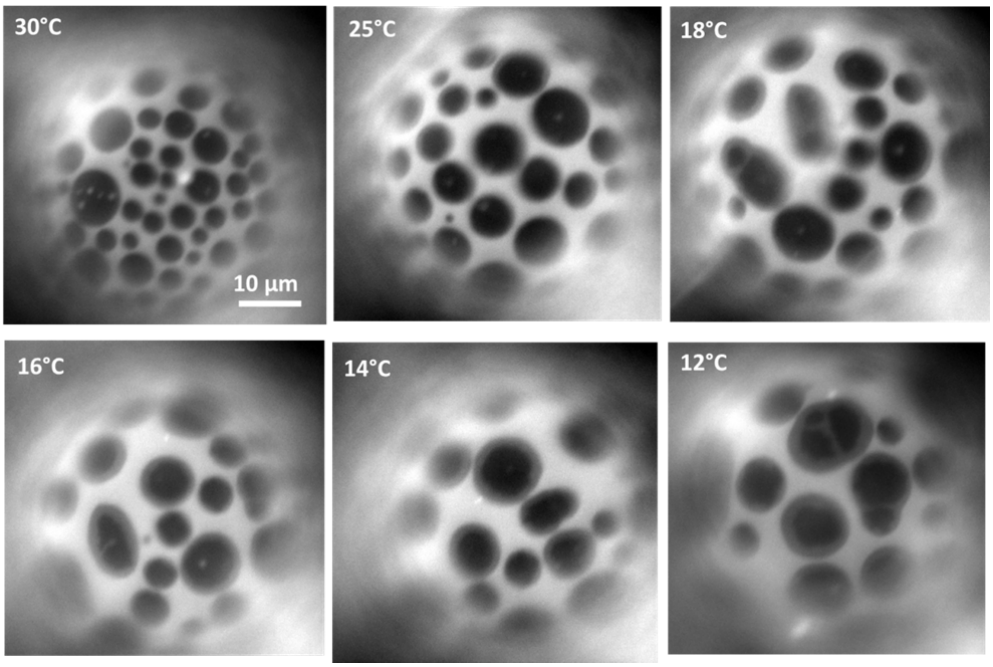


Fig S4: Example of the formation of the intermediate fluorescence intensity level for a DiPhyPC/bSM/Chol 1/1/1 vesicle not grabbed by a micropipette upon a decreasing temperature run.

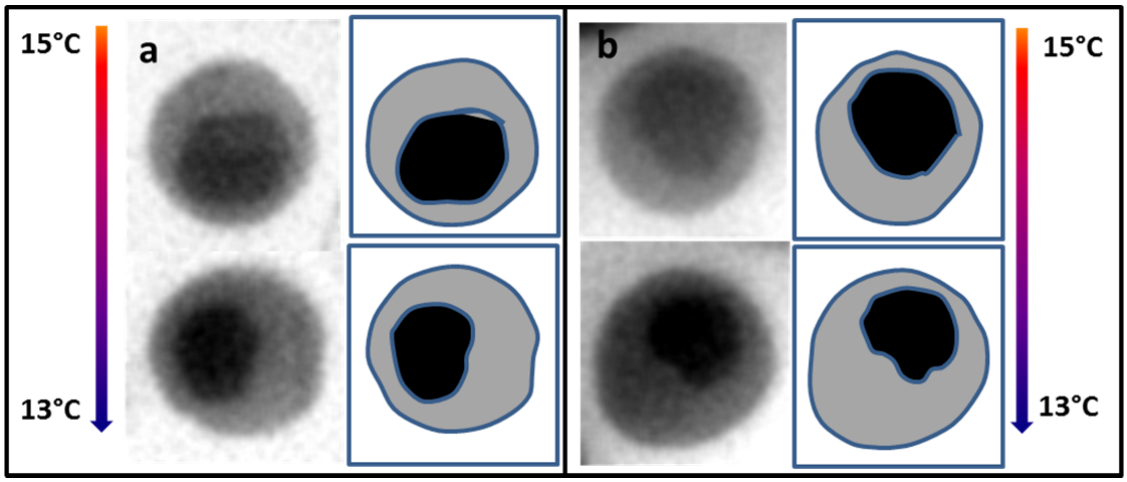


| | 15°C | | 13°C | |
|---|---|---|---|---|
| | Grey region | Black region | Grey region | Black region |
| a | 79 | 48 | 103 | 39 |
| b | 82 | 51 | 109 | 42 |

Fig. S5: Analysis of the area variation as a function of temperature for the darkest and the intermediate region in the case of two domains (a and b) from the sequence reported in Fig. 2 of the manuscript and Movie S1. Both the fluorescence images and schemes of how the domains have been calculated are reported. The Table reports the area of the different domains for two different temperatures (15°C and 13°C). The grey region is the region defined by the external border of the intermediate fluorescence level whereas the black region is the area of the region with the lowest fluorescence intensity level. The unit for area quantification is $\mu m^2$.

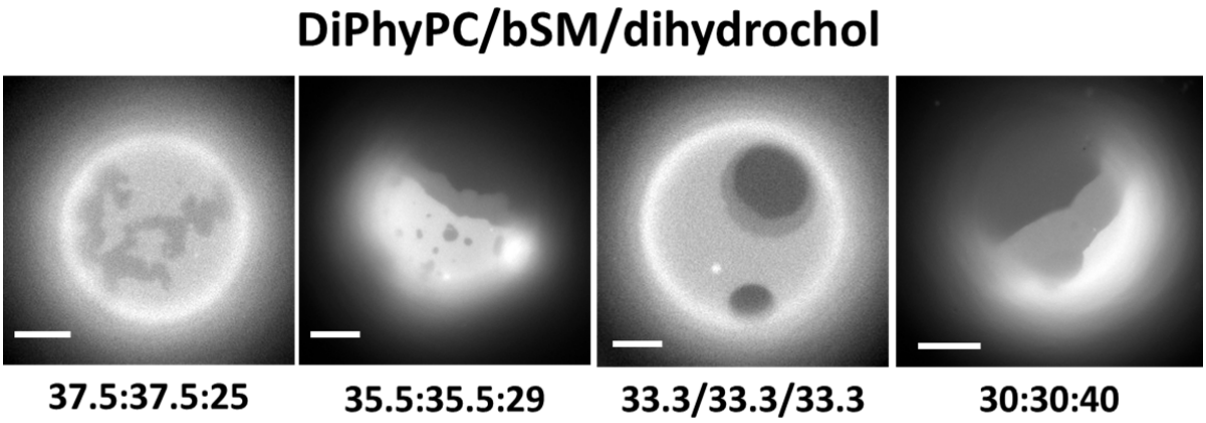


Fig. S6: We considered different molar proportions of the DiPhyPC/bSM/dihydrochol mixture. In particular, keeping an equal molar proportion between DiPhyPC and bSM (1:1) we changed the amount of cholesterol. We found that a low amount of cholesterol (~25%) easily produced the $S_o$ phase coexisting with the $L_d$ phase and the three different fluorescent intensities were never observed. For higher cholesterol concentrations (up to 40%) the coexistence of the three intensities was always observed with no evidence of a dependence of the percentage of GUVs in this state on the cholesterol amount. (Bar = 10 μm)

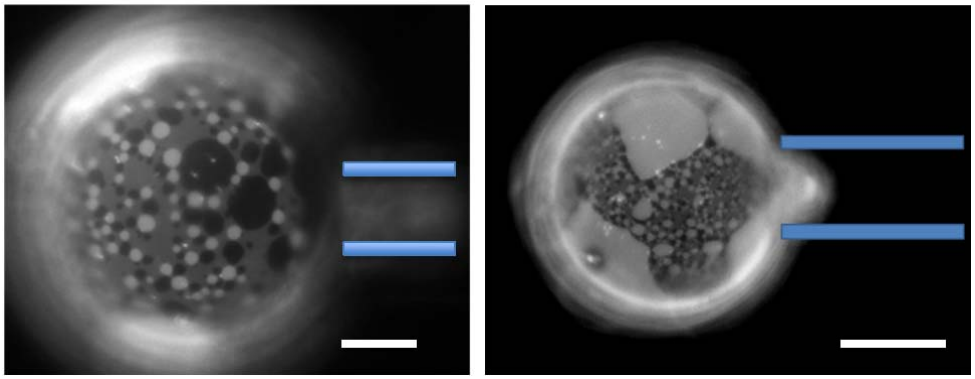

Fig. S7: Examples of other GUVs for which the application of the lateral tension by the MAT set-up induces the appearance in the intermediate fluorescence intensity level region of bright and dark round domains. The blue bars represent the position of the micropipette. (Bar = 10 μm)

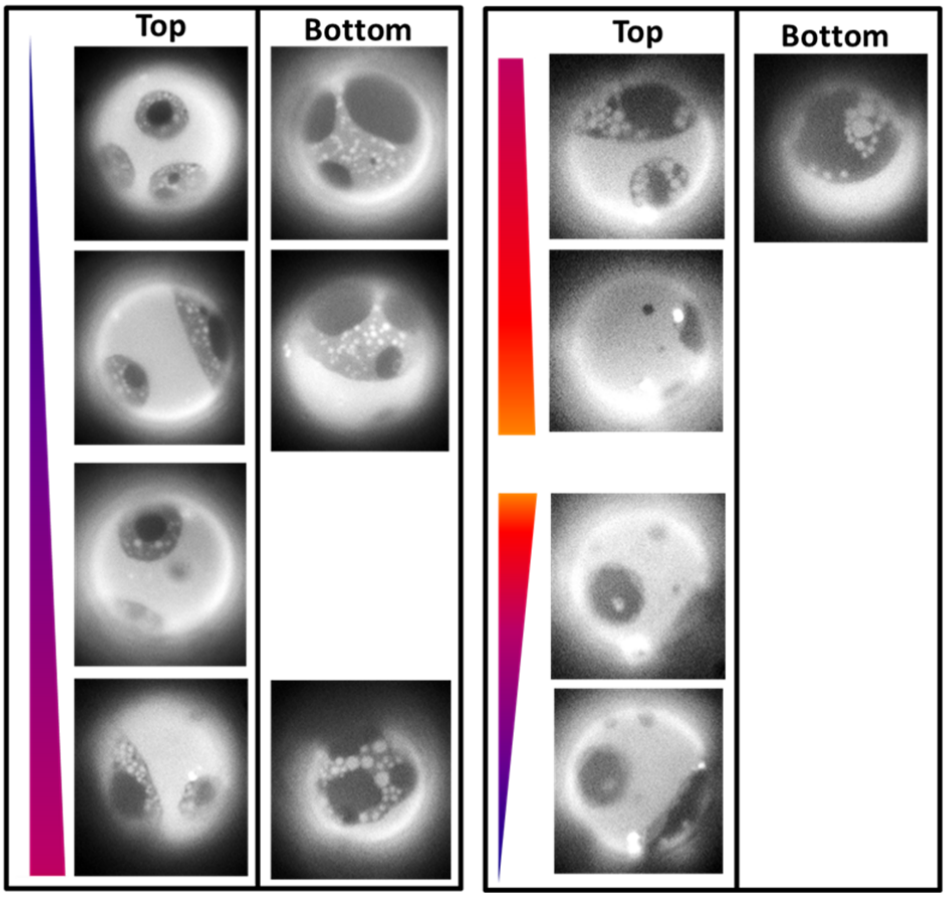


Fig. S8: Sequence of fluorescence microscopy images of a DiPhyPC/bSM/chol 1/1/ 1 GUV (+ 1% Texas Red-DHPE) upon a temperature cycle. The colored triangles and the arrows show the temperature variation trend. Couples of images have been reported when both the top and bottom surfaces of the GUVs have been captured

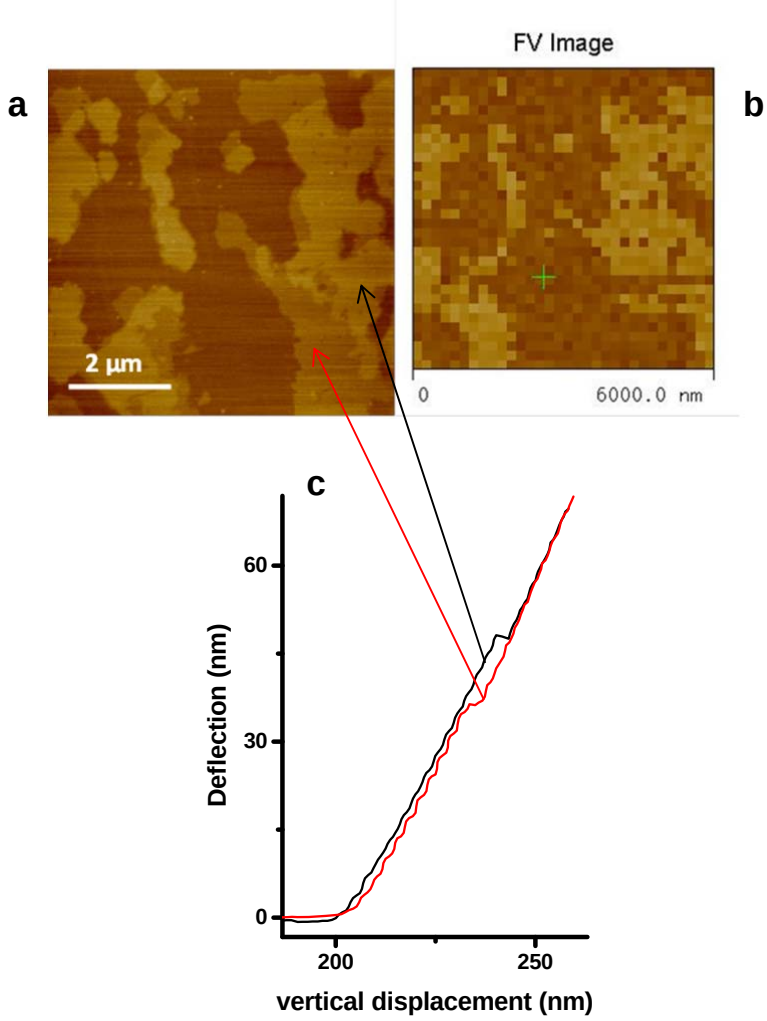


Fig. S9: a) Topography image of a DiPhyPC/bSM/Chol 1/1/1 SLB at 16°C; b) Force Volume image corresponding to the force spectroscopy analysis of the same region in a). The threshold value for the deflection has been chosen to show the punch-through force difference among the different domains; c) two examples of force curves coming from the regions pointed by the arrows.

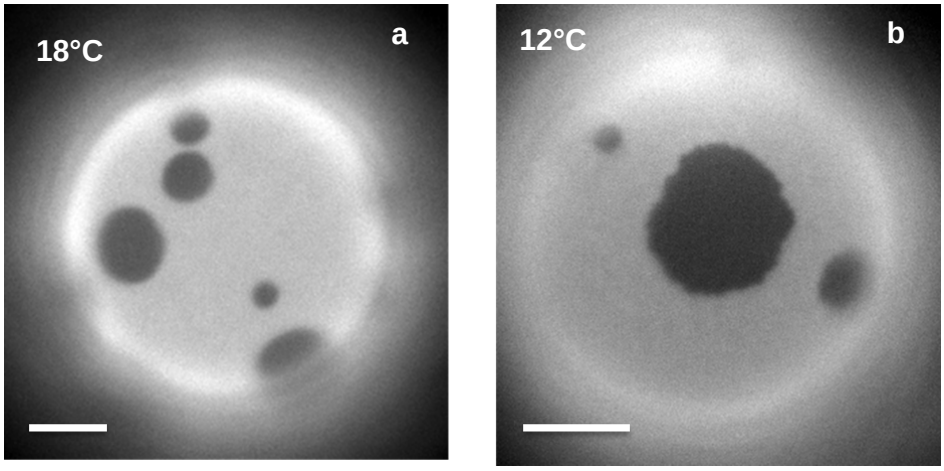


Fig. S10: Examples of fluorescence microscopy images of DiPhyPC/eggSM/chol 1/1/1 (+ 1% Texas Red-DHPE) GUVs. In no cases the presence of more than 2 fluorescence intensity levels has been observed. Bar = 10 µm.

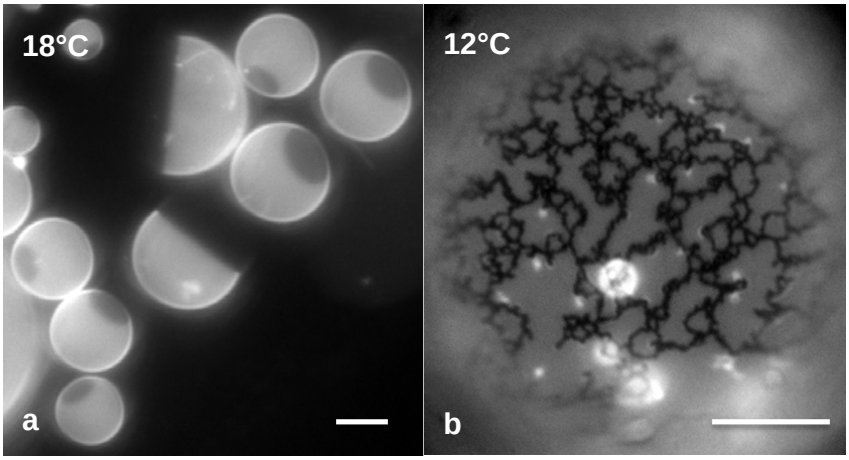


Fig. S11: Examples of fluorescence microscopy images of DiPhyPC/(18:0)SM/Chol 40/40/20 (+ 1% Texas Red-DHPE) GUVs. The presence of more than 2 fluorescence intensity levels has never been observed. Bar = 10 µm.

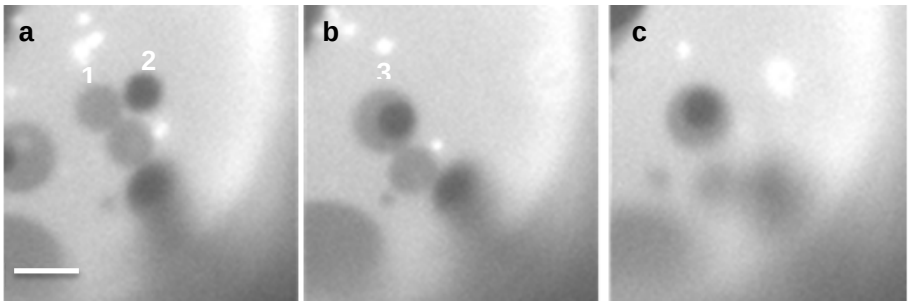


Fig. S12: The sequence shows what happens when a region with the darkest fluorescence intensity merges with an intermediate region. The darkest region is completely included in the intermediate region and the overall area of the domains at the end of the coalescence event is approximately equal to the sum of the two initially separated regions. This behavior is not in accordance with the confinement of the two different domains to the two opposite leaflets Quantitative analysis of the area of different domains upon coalescence: The area (in pixel$^2$) of domain 1 in a) is 168, for domain 2 we have 102. Upon merging of the two domains, the overall area of the formed domain (3) is 298. The fact that the area of the new domain is almost equal to the sum of the two initial domains points to the fact that the two domains span the overall bilayer thickness and they are not confined to a single leaflet. (Bar = 10 μm)

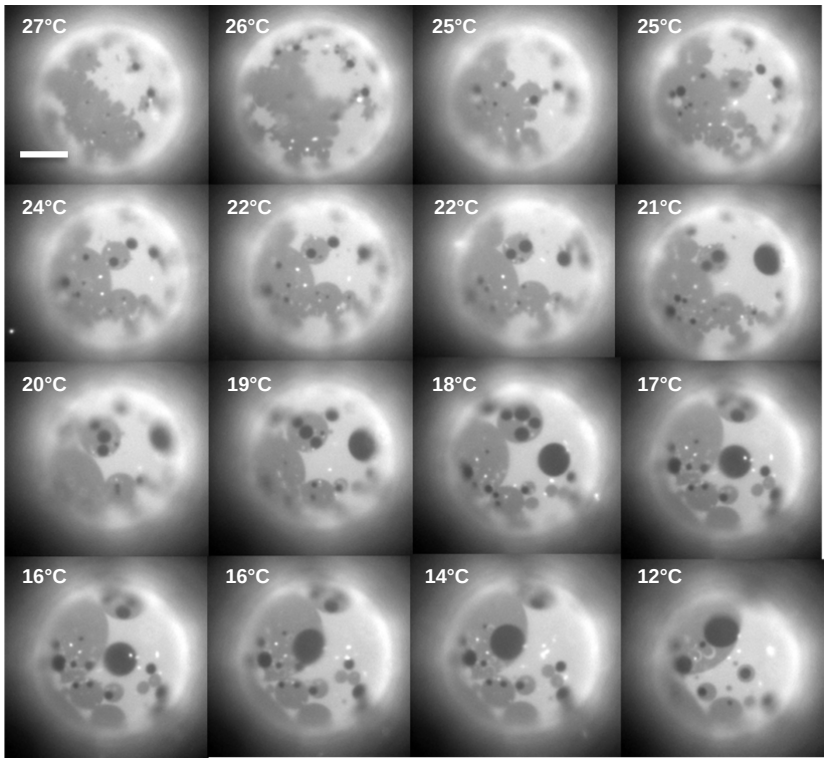


Fig. S13: Sequence of fluorescence microscopy images of a DiPhyPC/(24:1) SM/Chol + 0.5% DHPE Texas Red GUV as the temperature is decreased from 27°C to 12°C. The border between the brightest and the intermediate fluorescence intensity regions gradually gets more defined and regular and the darkest domains, once included inside a larger intermediate domain, get trapped in that position. The sequence corresponds to the vesicle shown in Fig. 7 of the manuscript. (Bar = 10 μm)

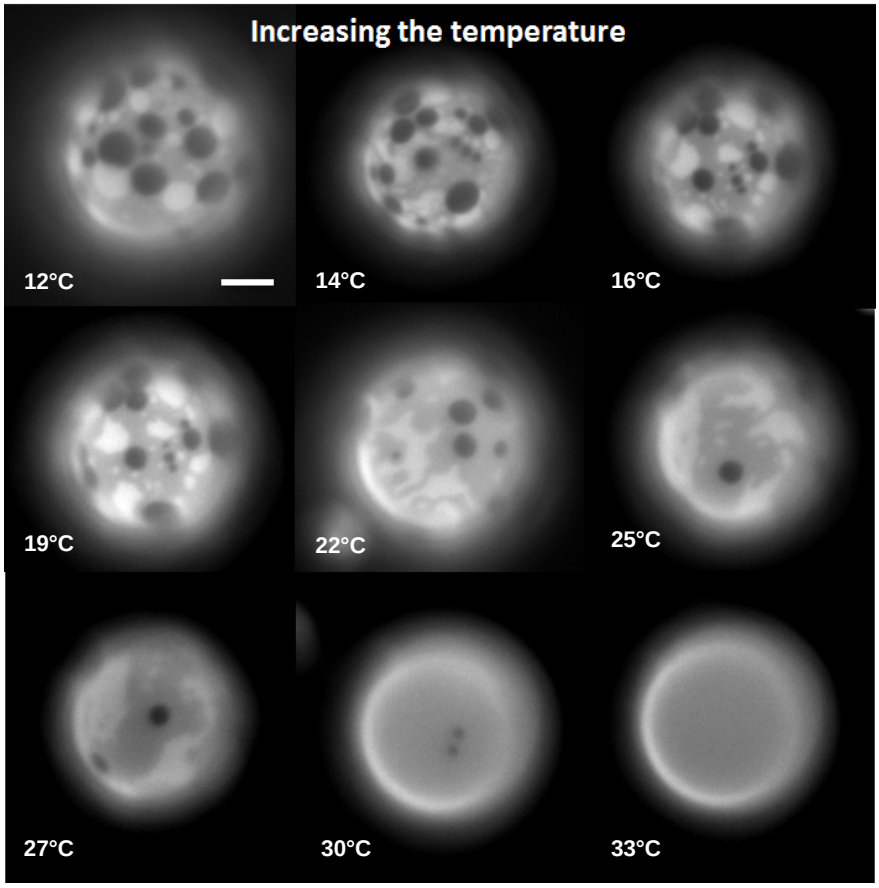


Fig. S14: Phase behavior of a DiPhyPC/(24:1)SM/Chol 1/1/1 (+ 0.5% Texas Red-DHPE) upon temperature increase. Bar = 10 µm.

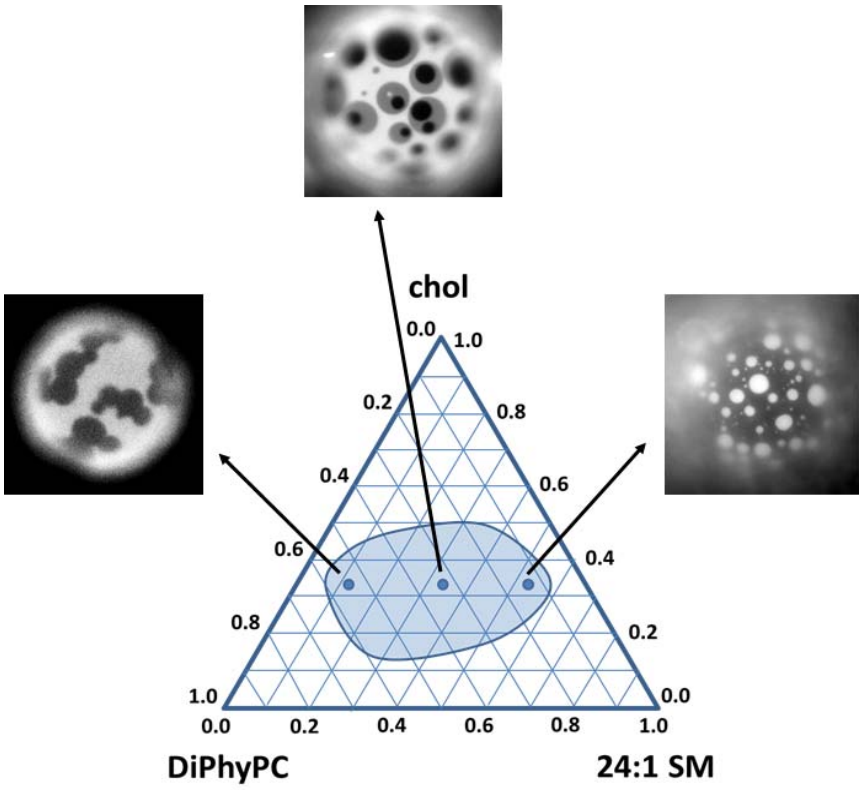


Fig. S15: Appearance of the different fluorescence intensity levels as a function of composition for the ternary mixture DiPhyPC/24:1 SM/chol + 1% Texas Red. The highest fraction of vesicles presenting three fluorescence intensity levels is obtained for a lipid composition with an approximately equal concentration of DiPhyPC and (24:1)SM.

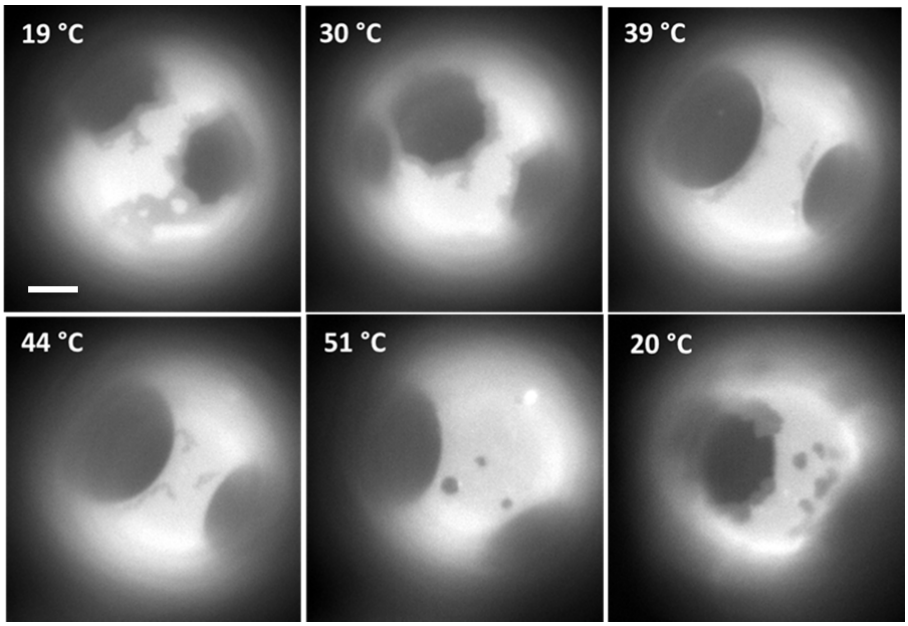


Fig. S16: Sequence of fluorescence microscopy images of a GUV composed by DiPhyPC/(24:0)SM/Chol 1/1/1 plus 1 % DHPE Texas Red. The vesicle has been exposed to a temperature cycle: from 19°C to 51°C and back. The presence of an intermediate fluorescence intensity level wetting the darkest domains is removed at 51°C and reappears at around 25°C. Bar = 10 µm.

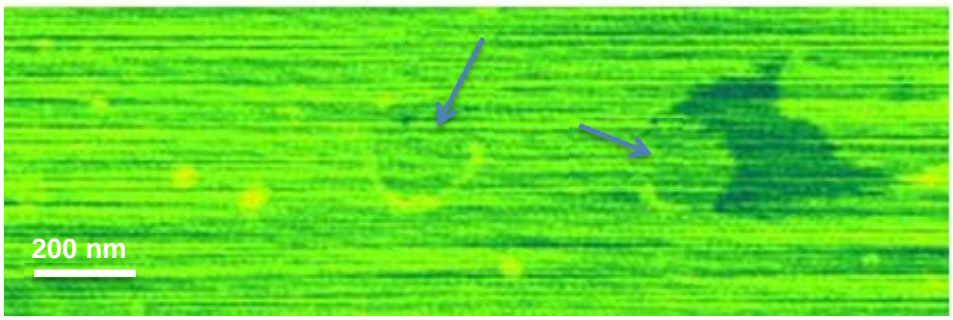


Fig. S17: Higher magnification of Fig. 8a with false colors to highlight the fact that the regions inside the arcs (arrows) have a different height (higher) with respect to the surrounding bilayer. In the false colors representation darkest regions are thicker.

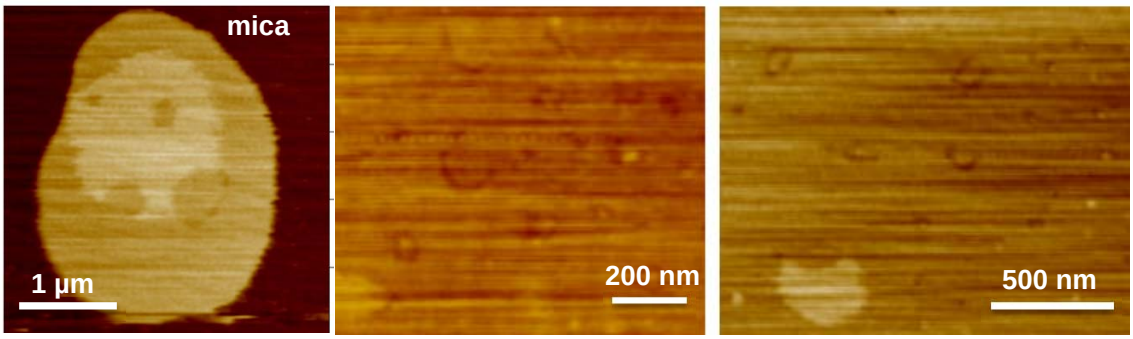


Fig. S18: AFM images of DiPhyPC/(24:1)SM/Chol 1/1/1 SLBs showing the presence of more than two height levels corresponding to the presence of more than two different domain thicknesses. The images have been acquired at a temperature of 12°C

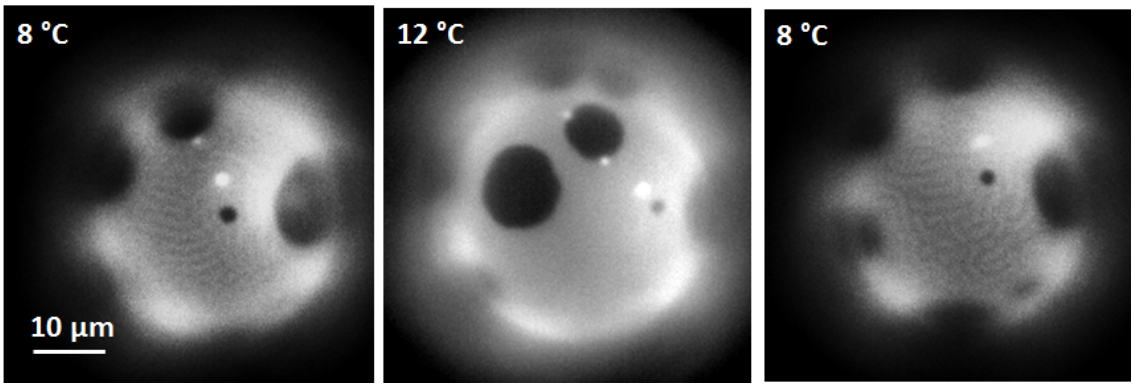


Fig. S19: Appearance of a modulated phase as a function of temperature for a DiPhyPC/(24:1)SM/Chol 1/1/1 +1% Texas Red DHPE GUV. The appearance and disappearance of the modulation is reversible.

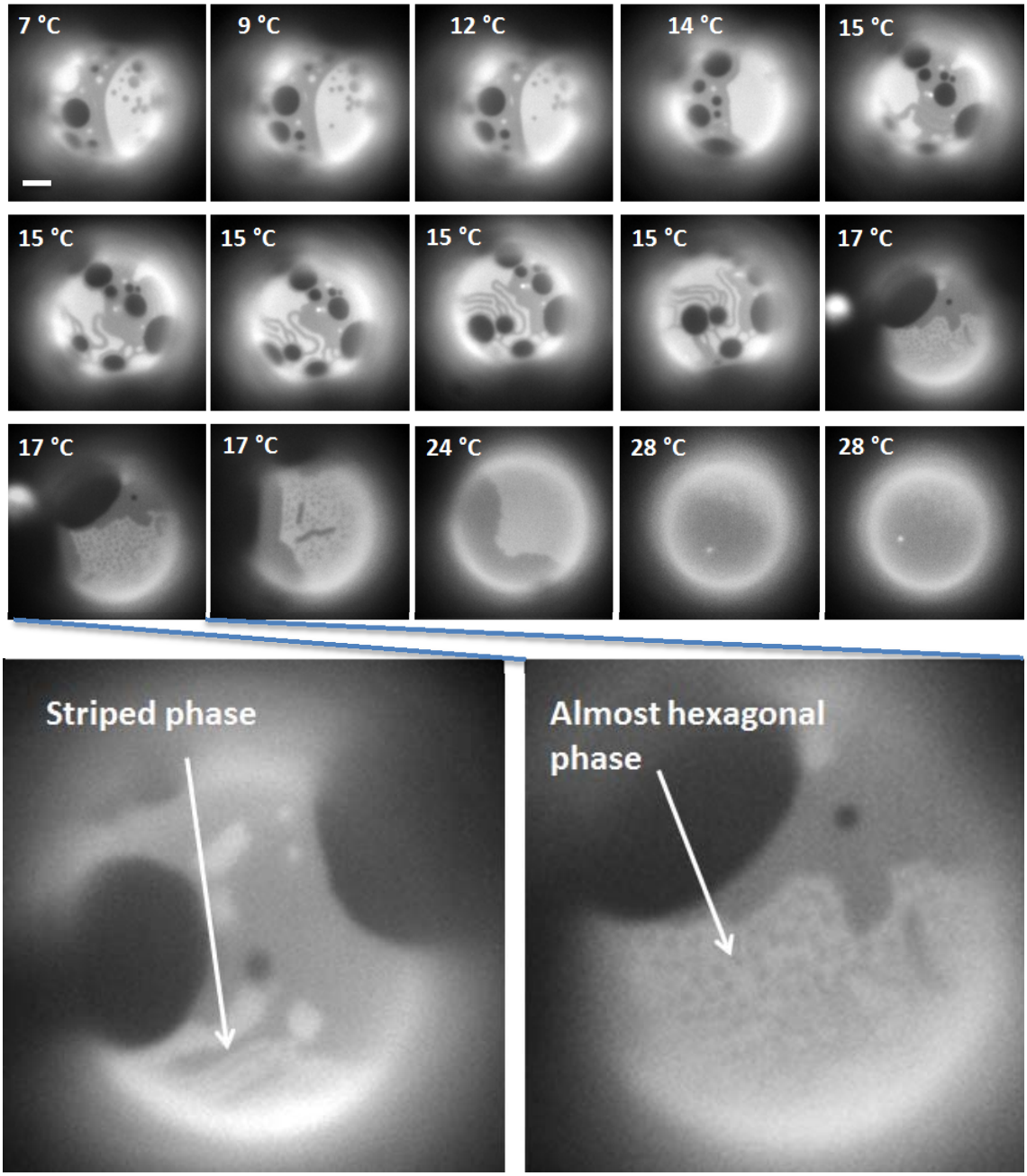


Fig. S20: Example of the appearance of striped domains upon temperature increase for a DiPhyPC/(24:1)SM/chol 1/1/1 + 1% Texas Red DHPE GUV. The striped domains appear after the decrease of the line tension between the domains with the highest fluorescence intensity and the domains with the intermediate intensity. Scale bar for the upper images = 10 µm.

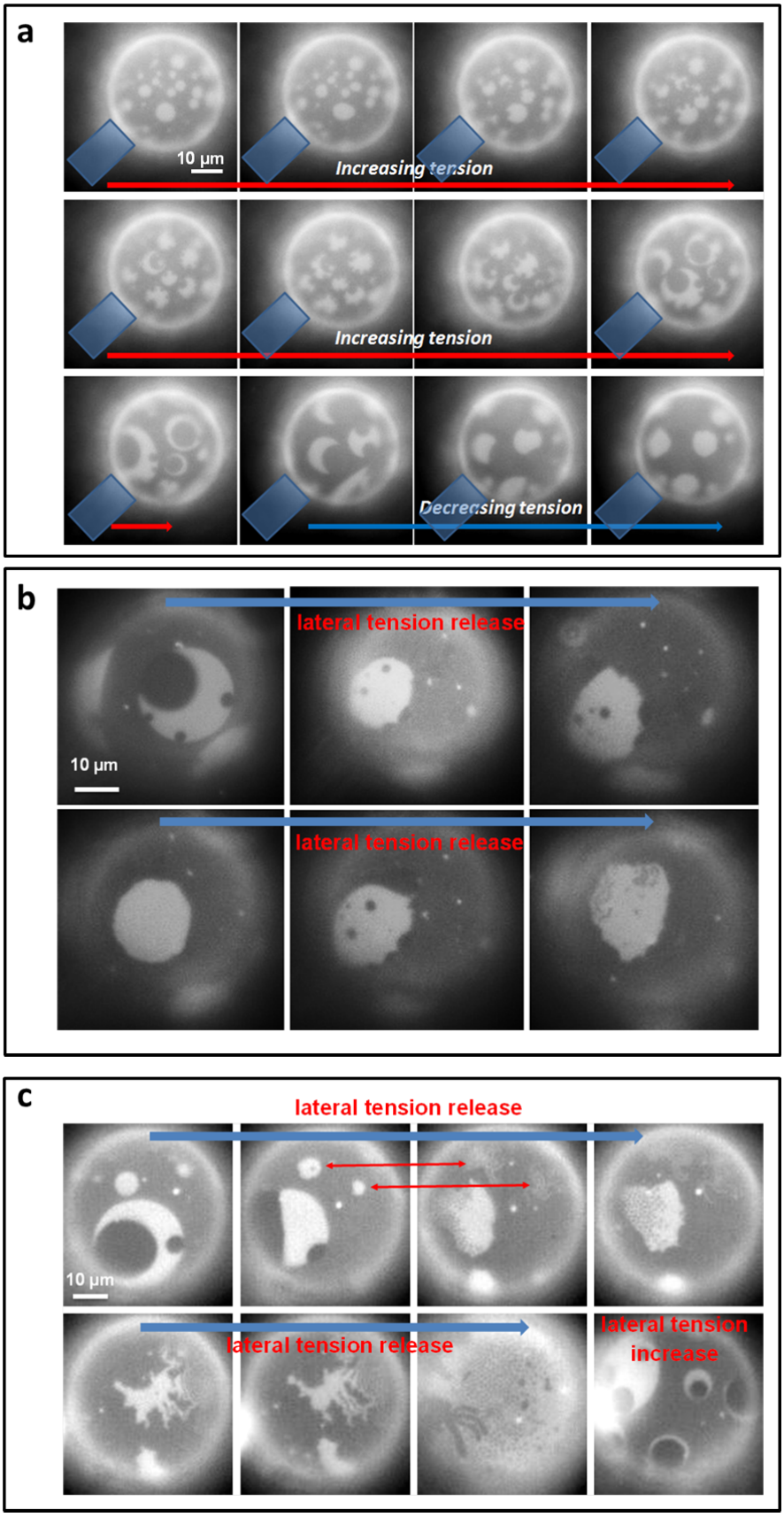


Fig. S21: a,b,c) Examples of shape changes of domains for DiPhyPC/(24:1)SM/Chol 1/1/1 (+ 1% Texas Red DHPE) GUVs upon an increase or release of the lateral tension obtained by a Micropipette Aspiration set-up at 15°C. The blue object in a) represents the position of the micropipette.

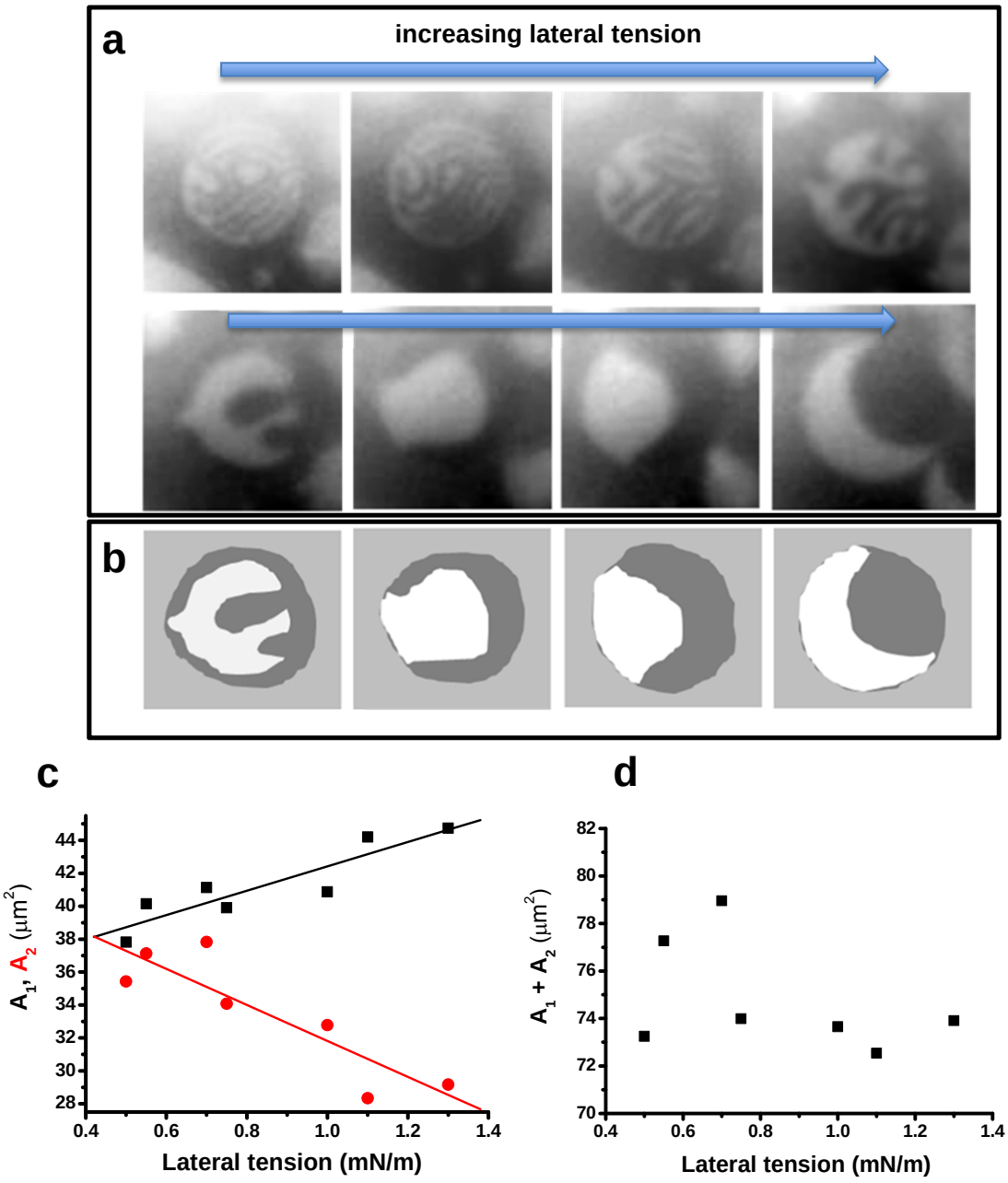


Fig. S22: a) Sequence of fluorescence microscopy images showing the detailed analysis of a domain in Fig. 10. b) Schematic representation of the domains corresponding to the second row in a); c) Quantitative analysis of the white (black squares) and dark grey (red dots) regions as a function of the applied lateral tension; d) Sum of the dark grey and white regions as a function of the applied lateral tension.

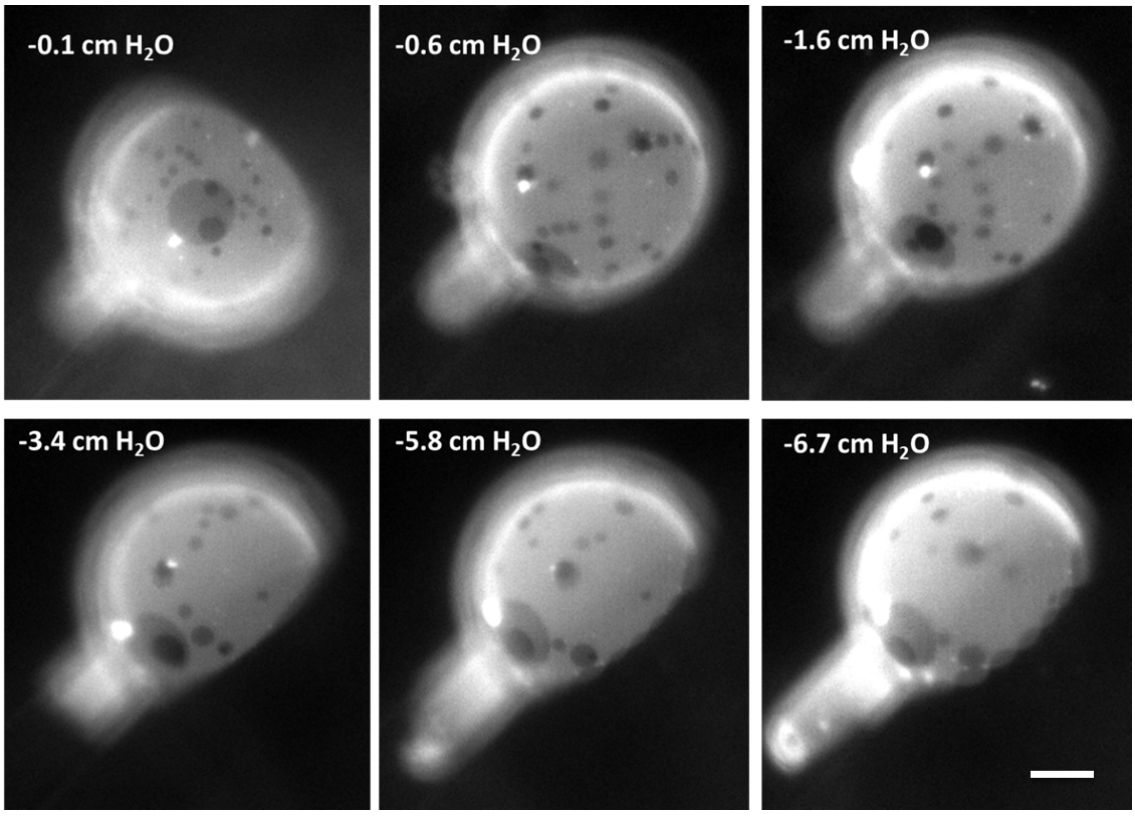


Fig. S23: Effect of the lateral tension on the shape of domains for a DiPhyPC/(24:1)SM/Chol 1/1/1 (+1% Texas Red DHPE) in the case of Type II domains of Fig. 5. Upon a lateral tension increase little effect is observed on the shape of the domains. Bar = 10 μm.

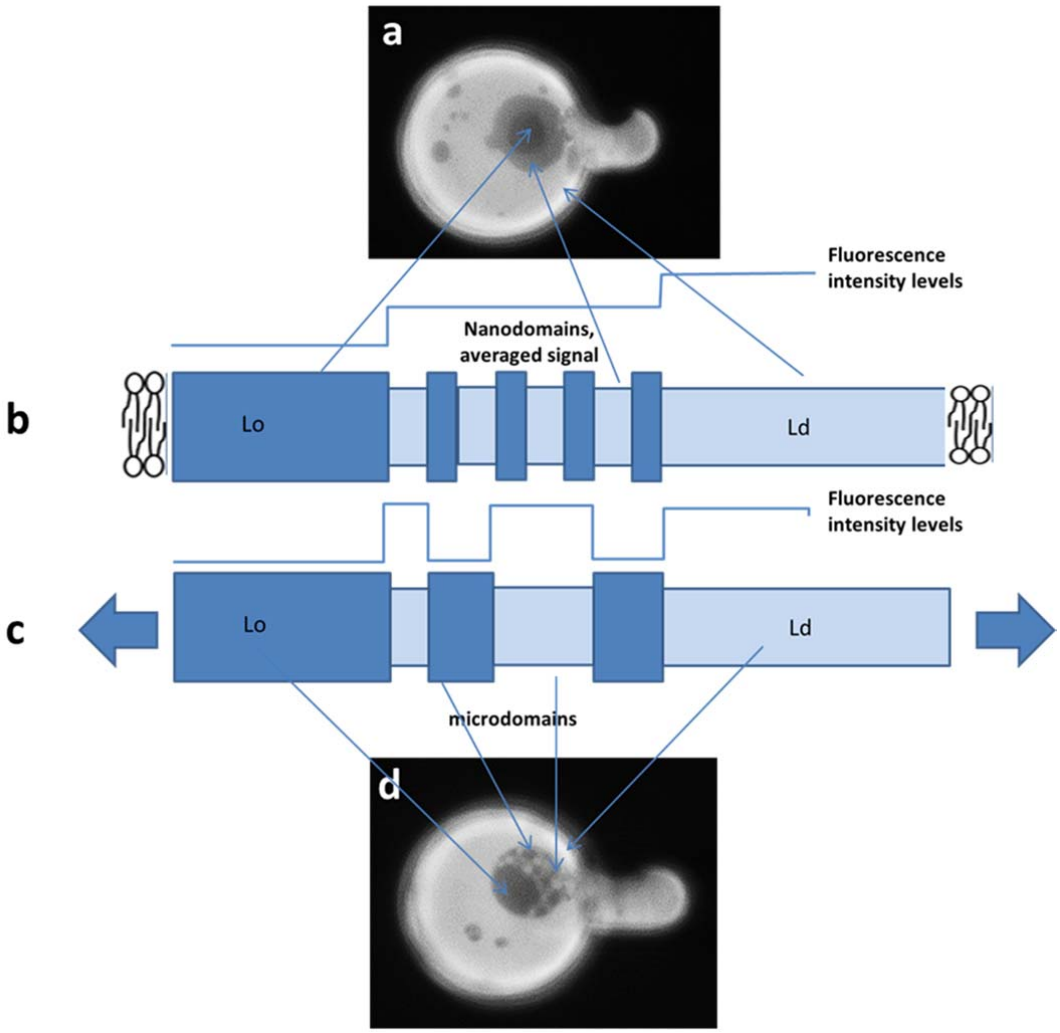


Fig. S24: Scheme of a possible interpretation for the appearance of the intermediate fluorescence intensity level upon temperature decrease and of its removal in favor of black (the darkest fluorescence level) and white (the highest fluorescence level) regions upon an increase of the lateral tension.

# Line tension measurement

## Theory

The line tension can be estimated from the (Fast) Fourier analysis of the $L_o$ and $L_d$ domains' contour fluctuations. The method is illustrated in detail in refs. [1], [2] but we provide here a brief account.

Given a selected domain, its image is recorded in time with a sufficient number of frames; for each frame, the radius as a function of the angle, $r(\vartheta)$, is extracted and the associated $n$-mode amplitudes $|u_n|$ are derived either by direct analysis or from the autocorrelation function $c(\delta) = \langle r(\vartheta)r(\vartheta+\delta)\rangle_\vartheta = (R_0^2/2)\Sigma_n |u_n|^2 \cos(n\delta)$, being $R_0$ the radius of a circle with the same area of the analyzed domain. The averages of the square amplitudes yield the line tension $\sigma$ through [1]

$$\sigma = \frac{k_B T}{\pi R_0 (n^2-1)\langle |u_n|^2 \rangle} ,$$

where $k_B T$ is the thermal energy.

A 40x objective lens has been used, and the pixel size approximately corresponds to 114 nm. The exposure times range from 20 to 30 ms and the cycle times from 30 to 50 ms (if we increase the cycle time up to 250 ms the obtained results are very similar). Being the number of images for each sequence in the order of 600, the overall acquisition time takes 18-30 s. The domains are selected following the criteria indicated in [1,2], namely:

- Their area must not exceed 1/5 of the total area of a GUV
- Their shape must be almost circular
- Their radius must be not less than 3 μm
- They must be planar and located at about the center of the GUV imaged surface
- Their area must remain constant during the whole acquisition time

Selection of GUVs with appropriate domains is performed using as low as possible light intensity to prevent photo-oxidation. The images are collected by fluorescence microscopy; then, discrete approximations of the domain contours are obtained by superposing a square mesh mask to the images, which are converted to binary afterwards (the ImageJ software was used).

The length $\Delta x_{lim}$ = 114 nm corresponding to the pixel size, poses a limit on the maximum mode number $n_{max}$ which makes sense to be analyzed: the wavelengths of the Fourier components (e.g. in the autocorrelation function) are $2^n$ submultiples of the fundamental wavelength $\lambda_1 \equiv 2\pi R_0$, so that it is readily found that $n_{max} = \log_2(\lambda_1/\Delta x_{lim})$. Contours of domains with approximately 3 μm radius can be analyzed up to the 6$^{th}$ mode.

The problem of photo-oxidation has been considered already in ref. [2] and it is addressed here because we used a fluorophore concentration significantly higher (~5 times) than in that work. To check the relevance of induced photo-oxidation on the domains, we partitioned the image sequence in four sub-sets made of the same number of frames. For each sub-set the line tension was estimated in order to reveal whether any systematic drift of $\sigma$ in time was detectable; our results did

not show any such tendency. Eventually, we analyzed the dependence of the line tension as a function of domain radius and, within errors, no influence on the domain size was observed.

## Results

We compared the value of the line tension in the case of domains for a well-known lipid mixture (DiPhyPC/DPPC/Chol) with the case of domains of Type I (see manuscript) for the DiPhyPC/(24:1) SM/Chol mixture which showed the maximum sensitivity to the applied lateral tension. Fig. S24 shows typical examples of the domains we analyzed.

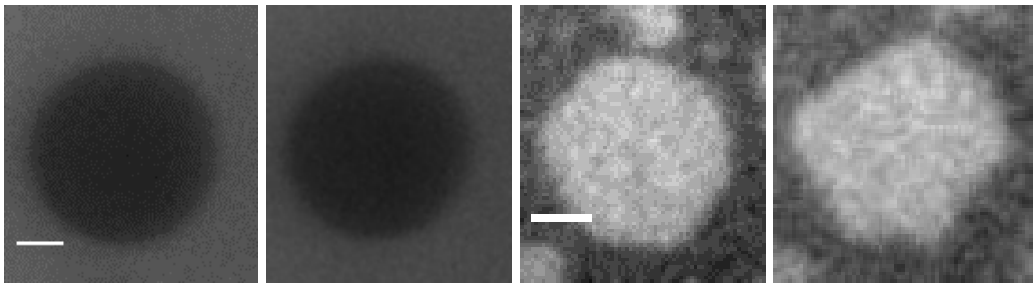

a) b) c) d)

Fig. S25: a) and b) represent a $L_o$ domain obtained from the DiPhyPC/DPPC/Chol mixture (1/1/1 molar ratio), as it appears in the initial and final frame of the analysis respectively . c) and d) represent a $L_d$ domain obtained from the DiPhyPC/(24:1) SM/Chol mixture (1/1/1 molar ratio), as it appears in the initial and final frame respectively. Bar = 2 μm

**Line tension components (Variance and mean amplitude):**

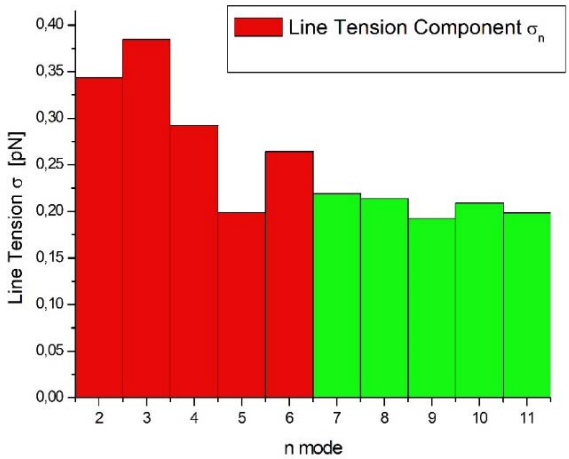


Fig. S26: Example of line tension estimate from different Fourier mode amplitudes as a function of mode number *n*. Only the first terms (up to the 6$^{th}$ mode) are relevant (red bars).

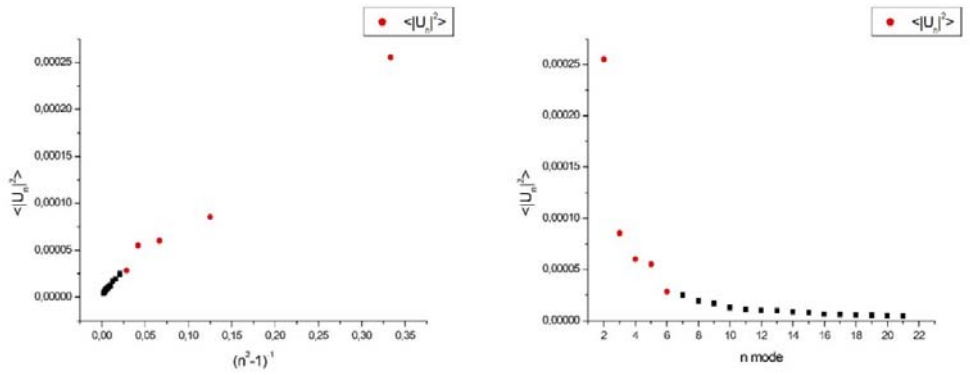


Fig. S27: Mean square amplitudes $\langle|u_n|^2\rangle$ of the autocorrelation function as functions of $(n^2-1)^{-1}$ (left) and mode number $n$ (right). Amplitudes from the 2nd to the 6th mode are plotted as red dots.

**Line tension subsets**

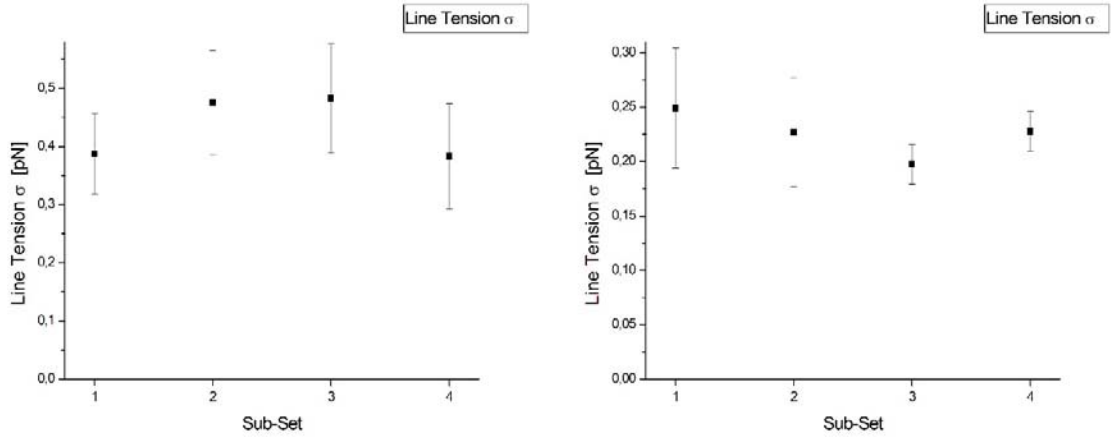


Fig. S28: Examples of estimated line tension for progressive sub-set number. The results do not show a significant dependence on the sub-sets; thus, the photo-oxidation process should be minimal.

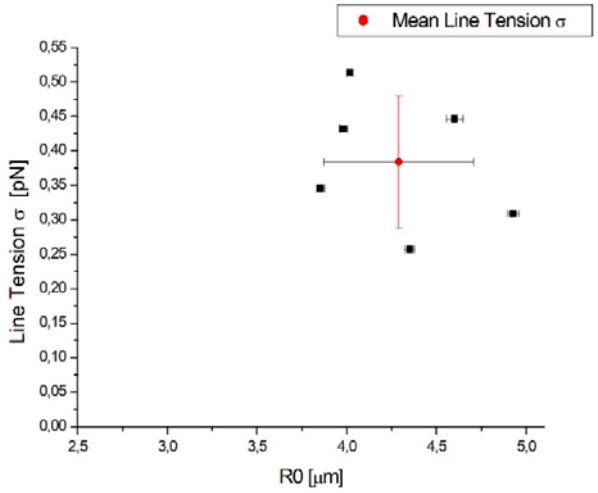


**Line tension as a function of domain radius**

Fig. S29: Line tension as a function of domain radius for six $L_o$ domains of a DiphyPC/DPPC/Chol 1/1/1 mixture. Only the domains with radius larger than 3 μm have been considered, as they allow to access a larger number of modes (up to the 6th one at least).

**Line tension comparison**

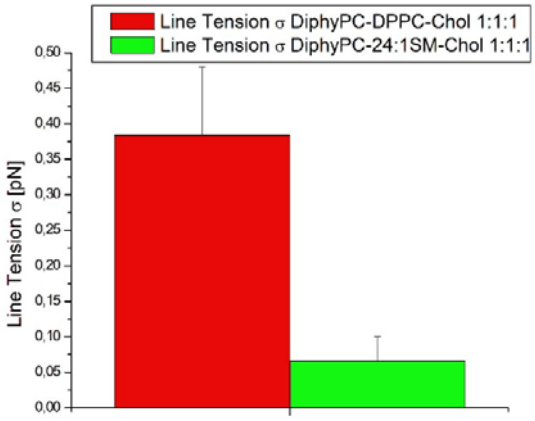


Fig. S30: Comparison of line tension estimates from $L_o$ domains of DiPhyPC/DPPC/Chol 1/1/1 mixture (red) and $L_d$ domains of DiPhyPC/(24:1) SM/Chol 1/1/1 mixture (green): The line tension for the domains in the first type of mixture (0.384 ± 0.096 pN) is larger than in the case of the second mixture (0.066 ± 0.035 pN).

**References**

[1] Esposito C, Tian A, Melamed S, Johnson C, Tee SY, Baumgart T., Flicker spectroscopy of thermal lipid bilayer domain boundary fluctuations. Biophys J. 2007 Nov 1;93(9):3169-81

[2] Usery RD, Enoki TA, Wickramasinghe SP, Weiner MD, Tsai WC, Kim MB, Wang S, Torng TL, Ackerman DG, Heberle FA, Katsaras J, Feigenson GW.,Line Tension Controls Liquid-Disordered + Liquid-Ordered Domain Size Transition in Lipid Bilayers. Biophys J. 2017 Apr 11;112(7):1431-1443.

## Movies' legends

**Movie S1**: Fluorescence microscopy movie of a DiPhyPC/bSM/Chol 1/1/1 (plus 1% Texas Red DHPE) vesicle undergoing a decreasing temperature ramp. The vesicle is grabbed by a micropipette (on the right of the vesicle, not visible in the fluorescence microscopy image). The temperature decreases from 50°C to 12°C. (see Figure 2 in the manuscript for other details).

**Movie S2**: Fluorescence microscopy movie of a DiPhyPC/bSM/Chol 1/1/1 (plus 1% Texas Red DHPE) vesicle showing the presence of three fluorescence intensity levels and undergoing an increase of the lateral tension at a constant temperature of 15°C. (See Figure 3 in the manuscript for other details).

**Movie S3**: Fluorescence microscopy movie of a DiPhyPC/(24:1)SM/Chol 1/1/1 (plus 1% Texas Red DHPE) vesicle at 15°C undergoing repetitive cycles of lateral tension increase and decrease. The lateral tension is increased by a micropipette aspiration set-up (the micropipette, not visible in the image, is positioned on the left of the vesicle at 45° with respect to the horizontal direction). (see Figure 10 in the manuscript for other details).

**Movie S4**: Another example of the same type of vesicle as in Movie S2. The vesicle undergoes a sequence of lateral tension increase and decrease. See Figure S20a for other details.

**Movie S5**: Another example of the same type of vesicle as in Movie S2. The vesicle undergoes a rapid lateral tension decrease. See Figure S20b for other details.